

All three-angle variants of Tsirelson’s precession protocol, and improved bounds for wedge integrals of Wigner functions

Lin Htoo Zaw^{1,*} and Valerio Scarani^{1,2}

¹Centre for Quantum Technologies, National University of Singapore, 3 Science Drive 2, Singapore 117543

²Department of Physics, National University of Singapore, 2 Science Drive 3, Singapore 117542

Tsirelson’s precession protocol is a nonclassicality witness that can be defined for both discrete and continuous variable systems. Its original version involves measuring a precessing observable, like the quadrature of a harmonic oscillator or a component of angular momentum, along three equally-spaced angles. In this work, we characterise all three-angle variants of this protocol. For continuous variables, we show that the maximum score \mathbf{P}_3^∞ achievable by the quantum harmonic oscillator is the same for all such generalised protocols. We also derive markedly tighter bounds for \mathbf{P}_3^∞ , both rigorous and conjectured, which translate into improved bounds on the amount of negativity a Wigner function can have in certain wedge-shaped regions of phase space. For discrete variables, we show that changing the angles significantly improves the score for most spin systems. Like the original protocol, these generalised variants can detect non-Gaussian and multipartite entanglement when applied on composite systems. Overall, this work broadens the scope of Tsirelson’s original protocol, making it capable to detect the nonclassicality and entanglement of many more states.

I. INTRODUCTION

For single-particle systems governed by Hamiltonians up to quadratic order, like a particle in free space or a harmonic oscillator, Ehrenfest’s theorem tells us that the dynamical equations of the mean value of observables are exactly the same for both quantum and classical theories [1]. Counter-intuitively, Tsirelson introduced a protocol for systems with uniformly-precessing coordinates—i.e. quadratures of a harmonic oscillator or coordinates undergoing spatial rotations—that can positively distinguish quantum systems from classical ones [2]. He showed that if a uniformly-precessing coordinate of a classical system is measured at a randomly-chosen $\theta \in \{0, 2\pi/3, 4\pi/3\}$, the probability P_3 that the coordinate is positive is constrained by the inequality $P_3 \leq \mathbf{P}_3^c = 2/3$. The nonclassicality of a quantum system can therefore be certified by preparing a suitable state of the system that violates this inequality. This protocol is semi-device independent, in that both the dynamics and coordinate measurements of the system are assumed to be well-characterised, but does not require the sequential measurements needed for Leggett–Garg inequalities [3], nor the simultaneous measurements needed for tests of noncontextuality [4].

For the quantum harmonic oscillator, the amount of violation of the classical bound is related to integrals of the Wigner function over wedge-shaped phase space regions. Using this relation, the maximum score \mathbf{P}_3^∞ of the quantum harmonic oscillator was upper-bounded by Tsirelson to be $\mathbf{P}_3^\infty < 1$ [2], and upper-bounded using Werner’s bounds of single-wedge Wigner integrals [5] to be $\mathbf{P}_3^\infty \leq 0.822\,607$ [6].

Tsirelson’s precession protocol has also been extended to spin angular momentum [6] and general theories [7]—

the former has recently been experimentally verified in the nuclear spin of antimony [8]. The protocol has also been shown to be useful for detecting non-Gaussian entanglement of coupled harmonic oscillators using only quadrature measurements [9], and genuine multipartite entanglement of spin ensembles using only measurements of total angular momentum [10]. Some generalisations of the original inequality have also been introduced: inequalities where only two of the three angles are equally-spaced [11], and so-called “Type I” and “Type II” inequalities that arise from facets of a constrained classical probability polytope [12]. Although Tsirelson did not study these generalisations, he alluded to them in a concluding remark that his upper bound $\mathbf{P}_3^\infty < 1$ holds even when the probing angles were not multiples of $2\pi/3$ [2].

In this work, we characterise all three-angle variants of Tsirelson’s precession protocol. In Sec. II, we define the protocols, discuss their symmetries, and show that the variants introduced in Refs. [11, 12] belong to this family. We first study the protocols on the quantum harmonic oscillator in Sec. III, where we show that all the variants achieve the same maximum score \mathbf{P}_3^∞ , albeit for different states. We also prove the rigorous bounds $0.709\,364 \leq \mathbf{P}_3^\infty \leq 0.730\,822$, much tighter than the previously known ones. These in turn lead to improved bounds for triple-wedge integrals over Wigner functions, tightening the fundamental limits on the amount of Wigner negativity that can be present in certain sectors of phase space. In Sec. IV, we study the protocols on spin angular momenta. The maximal violation for a given spin exhibit a triangular symmetry in the parameter space, leading to an improved score for many values of the spin and removing some awkward features observed when sticking to the original protocol [6]. Extrapolating the limiting behaviour of the spin score, we also give the conjectured bounds $0.709\,364 \leq \mathbf{P}_3^\infty \leq 0.709\,511$ on the score of the harmonic oscillator.

When applied to composite systems, the original precession protocol was proven to be a witness of non-

* Electronic mail: htoo@zaw.li

Gaussian entanglement for continuous variables [9], and of genuine multipartite entanglement for spin systems [10]. In Sec. V, we prove that this holds also for the generalised variants. Furthermore, we show that the separable bounds for the coupled harmonic oscillators are the same as those that were previously found with the original protocol, and that there are entangled states for both the oscillators and spin ensembles that can only be detected by a generalised protocol that is not the original one. Before the conclusion, we also briefly touch upon the precession protocol with more than three angles in Sec. VI. There, we identify the aspects of our results that are also applicable in the larger family of protocols, and provide heuristic strategies that simplify the task of finding maximally-violating states.

II. THREE-ANGLE PRECESSION PROTOCOLS AND THE CLASSICAL INEQUALITY

Tsirelson's precession protocol and its generalisations involve uniformly-precessing observables. A pair of observables $A_x(\theta)$ and $A_y(\theta)$ with a parametric dependence on θ are uniformly-precessing if they satisfy

$$\begin{pmatrix} A_x(\theta) \\ A_y(\theta) \end{pmatrix} = \begin{pmatrix} \cos \theta & \sin \theta \\ -\sin \theta & \cos \theta \end{pmatrix} \begin{pmatrix} A_x(0) \\ A_y(0) \end{pmatrix}. \quad (1)$$

Examples include the position $A_x(\theta) \propto X(t = \theta T/2\pi)$ and momentum $A_y(\theta) \propto P(t = \theta T/2\pi)$ of a harmonic oscillator with period T , and the angular momentum $A_x(\theta) = \hat{n}_\theta \cdot \vec{J}$ of a particle along the direction $\hat{n}_\theta = (\cos \theta, \sin \theta, 0)$, where \vec{J} is the angular momentum vector, with $A_y(\theta)$ similarly defined.

Each member of the family of three-angle variants of Tsirelson's precession protocol is defined for a choice of three probing angles $\{\theta_k\}_{k=0}^2$. Up to an arbitrary offset $\theta_k \rightarrow \theta_k - \theta_0$, the probing angles can be labelled $0 =: \theta_0 \leq \theta_1 \leq \theta_2 < 2\pi$. Without any loss of generality, each protocol is therefore fully specified by the vector $\vec{\theta} := (\theta_1, \theta_2)$.

The protocol for a given $\vec{\theta}$ is applied to a pair of uniformly-precessing observables $A_x(\theta)$ and $A_y(\theta)$, and involves many independent rounds. In each round,

1. The system is prepared in some state. The stability of the preparation is required to achieve a high score, but the validity of the protocol does not require the assumption that the state is the same in each round.
2. $k \in \{0, 1, 2\}$ is chosen with a procedure that is uncorrelated from the preparation. Here, we work in the limit of large samples, so the sampling distribution does not really matter as long as outcome probabilities can be estimated to the desired precision.
3. The coordinate $A_x(\theta_k)$ is measured: the score is +1 if $A_x(\theta_k) > 0$, 1/2 if $A_x(\theta_k) = 0$, or 0 if $A_x(\theta_k) < 0$.

The round ends when the system is measured, so it does not matter if the measurement is performed destructively or not. After many rounds, we calculate the average score $P(\vec{\theta})$ of the protocol

$$\begin{aligned} P(\vec{\theta}) &:= \frac{1}{3} \sum_{k=0}^2 \left\{ \Pr[A_x(\theta_k) > 0] + \frac{1}{2} \Pr[A_x(\theta_k) = 0] \right\} \\ &= \frac{1}{3} \sum_{k=0}^2 \langle \Theta[A_x(\theta_k)] \rangle, \end{aligned} \quad (2)$$

where $\Theta(x)$ is the Heaviside function

$$\Theta(x) = \begin{cases} 1 & \text{if } x > 0, \\ 1/2 & \text{if } x = 0, \\ 0 & \text{otherwise.} \end{cases} \quad (3)$$

The original precession protocol introduced by Tsirelson considered $\theta_k = 2\pi k/3$. Later generalisations of the protocol include the equally-spaced case $\theta_k = \theta_1 k$ with $\pi/2 \leq \theta_1 \leq \pi$ [11] and the Type I inequality with $\theta_k = 4\pi k/5$ up to an offset of the probing angle [12]. Meanwhile, Ref. [12] also introduced the Type II inequality, where they considered the quantity $\tilde{P} = \sum_{k=0}^2 (-1)^k \langle \Theta[A_x(2\pi k/5)] \rangle$, again defined up to an offset of the probing angles. With the relation $\Theta(x) + \Theta(-x) = 1$ and $-\exp(i\theta) = \exp[i(\theta + \pi)]$, we can rewrite $-\Theta[A_x(2\pi/5)] = \Theta[A_x(7\pi/5)] - 1$, and so $\tilde{P} = 3P(4\pi/5, 7\pi/5) - 1$. Hence, previously studied variants of Tsirelson's precession protocol are all members of this family of three-angle protocols.

In classical theory, the observables A_x and A_y take scalar values. Hence, the classical score is constrained by the inequality $P^c(\vec{\theta}) \leq \mathbf{P}^c(\vec{\theta})$, where

$$\mathbf{P}^c(\vec{\theta}) := \max_{A_x, A_y} \frac{1}{3} \sum_{k=0}^2 \Theta(A_x \cos \theta_k + A_y \sin \theta_k) \quad (4)$$

is the maximum score achievable in classical theory. For the original choice of angles $\vec{\theta}_3 := (2\pi/3, 4\pi/3)$, Tsirelson showed that $\mathbf{P}_3^c := \mathbf{P}^c(\vec{\theta}_3) = 2/3$ [2]. As there are quantum states that achieve the score $P_3 := P(\vec{\theta}_3) > \mathbf{P}_3^c$, nonclassicality can be certified by observing the violation of the classical inequality [2, 6].

Similarly, performing the protocol with angles $\vec{\theta}$ and observing $P(\vec{\theta}) > \mathbf{P}^c(\vec{\theta})$ certifies the nonclassicality of the system. This requires working out the dependence of the maximum classical score $\mathbf{P}^c(\vec{\theta})$ on the probing angles $\vec{\theta}$. Intuitively, if the probing angles are spread apart far enough, $A_x(\theta)$ has to cross the line $A_x = 0$ at least once, thus $\mathbf{P}^c = 2/3$; but if they are too close together, $A_x(\theta)$ can remain on $A_x > 0$ plane, thus $\mathbf{P}^c = 1$. Indeed, we formally prove in Appendix A1 that

$$\mathbf{P}^c(\vec{\theta}) = \begin{cases} 2/3 = \mathbf{P}_3^c & \text{if } \forall k : \theta_{k \oplus 3} \ominus_{2\pi} \theta_k \leq \pi, \\ 1 & \text{otherwise;} \end{cases} \quad (5)$$

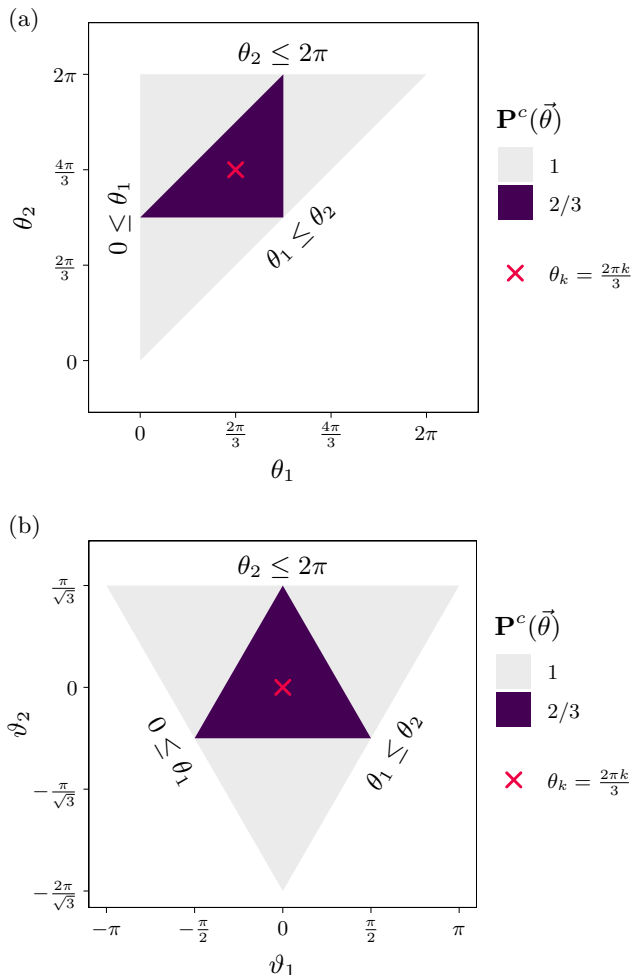


FIG. 1. Maximum classical score with respect to (a) $\vec{\theta}$ and (b) $\vec{\vartheta}$. The score invariance under the equivalent probing times given in Eq. (6) appear in the $\vec{\vartheta}$ coordinate as $2\pi/3$ rotations around the origin in (b).

where $x \oplus_m y = (x \pm y) \bmod m$ are addition and subtraction modulo m . The maximum classical score $\mathbf{P}^c(\vec{\theta})$ is plotted for the full parameter space against $\vec{\theta}$ in Fig. 1(a).

Note also that the probing angles

$$\begin{aligned} \{0, \theta_1, \theta_2\} &\leftrightarrow \{-\theta_1, 0, \theta_2 - \theta_1\} \bmod 2\pi \\ &\leftrightarrow \{-\theta_2, \theta_1 - \theta_2, 0\} \bmod 2\pi \end{aligned} \quad (6)$$

are equivalent up to an offset $\theta_{k_0} \in \{\theta_k\}_{k=0}^2$. As such, it is more illustrative to plot the parameter space with alternate coordinates $\vec{\vartheta}$, defined as

$$\vec{\vartheta} := \begin{pmatrix} 1 & -1/2 \\ 0 & \sqrt{3}/2 \end{pmatrix} (\vec{\theta} - \vec{\theta}_3). \quad (7)$$

In this coordinate, the equivalences in Eq. (6) become symmetry transformations

$$\vec{\vartheta} \leftrightarrow \mathcal{R}_{\frac{2\pi}{3}}^{-1} \vec{\vartheta} \leftrightarrow \mathcal{R}_{\frac{2\pi}{3}} \vec{\vartheta}, \quad (8)$$

where $\mathcal{R}_\theta = \begin{pmatrix} \cos \theta & -\sin \theta \\ \sin \theta & \cos \theta \end{pmatrix}$ is the rotation matrix in two dimensions. These alternate coordinates are again used to plot $\mathbf{P}^c(\vec{\theta})$ in Fig. 1(b).

For the rest of the paper, we shall use both $\vec{\theta}$ and $\vec{\vartheta}$ interchangeably. $\vec{\theta}$ is favoured when referring to the actual probing angles to be used when performing the protocol, while $\vec{\vartheta}$ is favoured when visualising quantities in the full parameter space, as it better reflects the symmetries and geometric features of the protocol.

III. QUANTUM HARMONIC OSCILLATOR

In natural units, the quantum harmonic oscillator is governed by the Hamiltonian $H = (X^2 + P^2)/2$, where the position X and momentum P satisfy the canonical commutation relation $[X, P] = i$. The evolution of X in time θ —equivalently the θ -quadrature of a bosonic field—is given by $X(\theta) = e^{iH\theta} X e^{-iH\theta} = X \cos \theta + P \sin \theta$.

As such, we can perform the precession protocol with the position of the quantum harmonic oscillator, where the maximum achievable score $\mathbf{P}^\infty(\vec{\theta})$ is

$$\mathbf{P}^\infty(\vec{\theta}) := \max_\rho \frac{1}{3} \sum_{k=0}^2 \text{tr} \{ \rho \Theta[X(\theta_k)] \} =: \text{maxeig} [Q^\infty(\vec{\theta})], \quad (9)$$

where $3Q^\infty(\vec{\theta}) := \sum_{k=0}^2 \Theta[X(\theta_k)]$ and $\text{maxeig}(A)$ is the largest eigenvalue of A .

While it was known that there are states of the quantum harmonic oscillator that violate some of the generalised precession protocols, an open question remained on whether a larger violation is possible by changing the probing time [12].

Since no violation of the classical bound is possible when $\mathbf{P}_3^c = 1$, let us focus on the subset $\Delta := \{\vec{\theta} : \mathbf{P}^c(\vec{\theta}) = 2/3\}$ of the parameter space, which corresponds to the inner purple triangle in Fig. 1. In Appendix A2, we show that the generalised protocols are related to the original one for $\vec{\theta} \in \Delta$ as

$$Q^\infty(\vec{\theta}) = \begin{cases} \frac{2}{3} U(\vec{\theta}) \Theta(X) U^\dagger(\vec{\theta}) & \text{if } \exists k : \theta_{k \oplus_3 1} \ominus_{2\pi} \theta_k = \pi \\ U(\vec{\theta}) Q_3 U^\dagger(\vec{\theta}) & \text{otherwise,} \end{cases} \quad (10)$$

where $U(\vec{\theta})$ is a symplectic unitary composed of squeeze and phase shift operations. Since unitary transformations leave eigenvalues invariant, Eq. (10) implies that $\mathbf{P}^\infty(\vec{\theta}) = \mathbf{P}^\infty(\vec{\theta}_3) =: \mathbf{P}_3^\infty$ if $\vec{\theta}$ is in the interior of Δ , while $\mathbf{P}^\infty(\vec{\theta}) = \mathbf{P}_3^c$ if $\vec{\theta}$ is on the boundary of Δ . This dependence of $\mathbf{P}^\infty(\vec{\theta})$ on $\vec{\theta}$ is plotted in Fig. 2.

This means that \mathbf{P}_3^∞ is the maximum achievable by the quantum harmonic oscillator for any choice of three angles, including those that define previously proposed generalisations. This maximum will however be achieved by different states: as announced, modifying the probing angles broadens the usefulness of the protocol. We

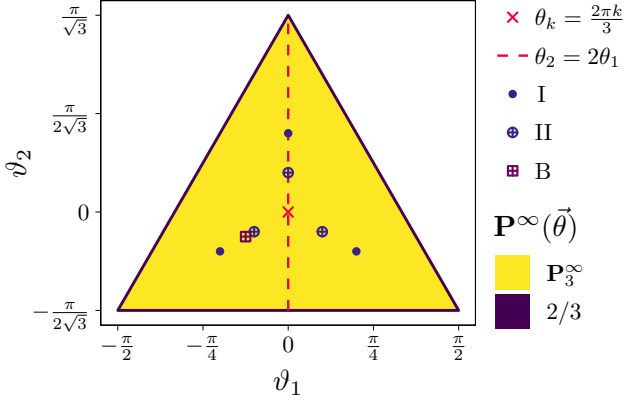


FIG. 2. Maximum scores $\mathbf{P}^\infty(\vec{\theta})$ for the quantum harmonic oscillator within the region where $\mathbf{P}^c < 1$ (compare to Fig. 1). The score is \mathbf{P}_3^∞ in the interior and \mathbf{P}_3^c along the boundary. The red cross (\times) marks the original protocol with probing angles $\theta_k = 2\pi k/3$ [2], while the red dashed lines (--) mark the equally-spaced protocol $\theta_k = \theta_1 k$ [11]. Up to a constant offset and a rescaling of $\mathbf{P}^\infty(\vec{\theta})$, the family of three-angle precession protocols also contains the Type I (\bullet) and II (\oplus) inequalities introduced in Ref. [12], and also provide bounds to the degree of quantum advantage in probability backflow and quantum projectiles [13, 14] labelled as “B” (\boxplus) in the figure.

also note that bounds of quantum advantages in other mechanical tasks, like probability backflow and quantum projectiles [13, 14], can also be found to be special cases of $\mathbf{P}_3(\vec{\theta})$, as labelled in Fig. 2.

A. Relation to Negativity Volume and Wedge Integrals of Wigner Functions

An alternate characterisation of continuous variable states is provided by the Wigner function, defined as [15]

$$W_\rho(x, p) := \frac{1}{2\pi i} \text{tr} \left(\rho e^{i\frac{\pi}{2}[(X-x)^2 + (P-p)^2]} \right), \quad (11)$$

which has the property that for any function $g(x)$,

$$\begin{aligned} & \langle g(X \cos \theta + P \sin \theta) \rangle \\ &= \iint dx dp g(x \cos \theta + p \sin \theta) W_\rho(x, p). \end{aligned} \quad (12)$$

Therefore, the Wigner function acts like a probability density function of x and p , although it is only a *quasiprobability* distribution as X and P are not jointly measurable in quantum theory. Nonetheless, it allows us to simultaneously study the classical and quantum harmonic oscillator in terms of an initial (quasi)probability distribution $F(x, p)$, where $F(x, p)$ is a joint probability density function in the classical case and $F(x, p) = W_\rho(x, p)$ in the quantum case. Then, the score $P(\vec{\theta})$

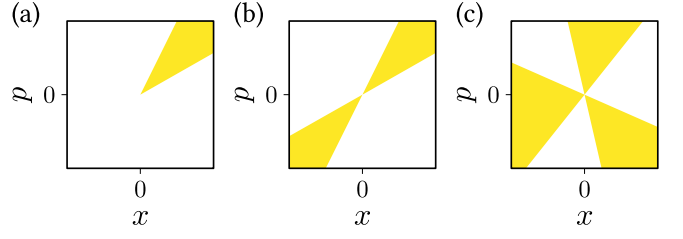


FIG. 3. The (a) single Ω_1 , (b) double Ω_2 , and (c) triple Ω_3 (equivalently Ω_\pm in Eq. (14)) wedges. The single wedge is a pointed sector stemming from the origin; while the double and triple wedges are, respectively, formed by two and three lines that cross the origin, and can also be seen as unions of single wedges. The exact angles do not matter, as different choices of angles are equivalent up to a symplectic transformation.

achieved by the oscillator is

$$\begin{aligned} P(\vec{\theta}) &= \sum_{k=0}^2 \frac{1}{3} \iint dx dp \Theta(x \cos \theta_k + p \sin \theta_k) F(x, p) \\ &= \mathbf{P}_3^c + \frac{1}{3} \left(\iint_{\Omega_+(\vec{\theta})} dx dp F(x, p) - 1 \right) \\ &= \mathbf{P}_3^c - \frac{1}{3} \iint_{\Omega_-(\vec{\theta})} dx dp F(x, p), \end{aligned} \quad (13)$$

where $\Omega_\pm(\vec{\theta})$ are the phase space regions

$$\begin{aligned} \Omega_\pm(\vec{\theta}) &= \{(x, p) : \forall k \in \{0, 1, 2\} : \\ & \theta_{k \oplus 3} 1 \mp \frac{\pi}{2} \leq \text{atan}(p, x) \leq \theta_k \pm \frac{\pi}{2}\}, \end{aligned} \quad (14)$$

which are illustrated in Fig. 3(c).

If $F(x, p)$ satisfies the properties of a joint probability density, that is if $0 \leq \iint_\omega dx dp F(x, p) \leq 1$ for every phase space region ω , then $|\frac{1}{2} - \iint_\omega dx dp F(x, p)| \leq \frac{1}{2}$ and Eq. (13) implies that $P(\vec{\theta}) \leq \mathbf{P}_3^c$. Therefore, the violation of the classical bound can be understood as the impossibility of assigning a classical probability distribution to x and p . A quantification of this impossibility is the Wigner negativity volume [16]

$$\begin{aligned} \mathcal{N}_V(\rho) &:= - \iint dx dp \Theta[-W_\rho(x, p)] W_\rho(x, p) \\ &= \frac{1}{2} \iint dx dp [|W_\rho(x, p)| - W_\rho(x, p)], \end{aligned} \quad (15)$$

which is a measure of nonclassicality in the resource theories of non-Gaussianity and Wigner negativity [17, 18].

The amount of violation of the precession protocol can therefore be interpreted as the lower bound for the negativity volume, since rearranging the last line of Eq. (13) gives $3P(\vec{\theta}) - 3\mathbf{P}_3^c \leq \mathcal{N}_V(\rho)$.

We can also rearrange Eq. (13) to

$$\left| \frac{1}{2} - \iint_{\Omega_{\pm}(\bar{\theta})} dx dp W_{\rho}(x, p) \right| = \frac{P(\bar{\theta}) - \frac{1}{2}}{2(\mathbf{P}_3^c - \frac{1}{2})} \leq \frac{\mathbf{P}_3^{\infty} - \frac{1}{2}}{2(\mathbf{P}_3^c - \frac{1}{2})}, \quad (16)$$

so the maximum quantum score \mathbf{P}_3^{∞} also fundamentally bounds integrals of Wigner functions over certain phase space regions. In fact, integrals over $\Omega_{\pm}(\bar{\theta})$ take the form of wedge integrals over phase space regions: these include the (single) wedge $\Omega_1 = \{(x, p) : \theta_1 \leq \text{atan}(p, x) \leq \theta_2\}$ and the double wedge $\Omega_2 = \{(x, p) : \theta_1 \leq \text{atan}(p, x) \leq \theta_2 \wedge \theta_1 \leq \text{atan}(p, x) - \pi \leq \theta_2\}$, both for $\theta_1 < \theta_2$, the latter so called because it is a union of two wedges. Both are illustrated in Fig. 3. Bounds for the single and double wedge integrals have been worked out to be [5, 19]

$$\begin{aligned} \sup_{\rho} \left| \frac{1}{2} - \iint_{\Omega_1} dx dp W_{\rho}(x, p) \right| &\approx 0.655\,940, \\ \sup_{\rho} \left| \frac{1}{2} - \iint_{\Omega_2} dx dp W_{\rho}(x, p) \right| &\approx 0.736\,824. \end{aligned} \quad (17)$$

Analogously, $\Omega_3 = \Omega_{\pm}$ is a union of three wedges and therefore a ‘‘triple wedge’’, for which

$$\sup_{\rho} \left| \frac{1}{2} - \iint_{\Omega_3} dx dp W_{\rho}(x, p) \right| = \frac{\mathbf{P}_3^{\infty} - \frac{1}{2}}{2(\mathbf{P}_3^c - \frac{1}{2})}. \quad (18)$$

B. Improved Rigorous Bounds

Prior to this work, the best known rigorous bounds of the maximum quantum score were [6]

$$0.708\,741 \leq \mathbf{P}_3^{\infty} \leq 0.822\,607 =: \mathbf{P}_3^{\geq\text{-old}}. \quad (19)$$

In particular, $\mathbf{P}_3^{\geq\text{-old}}$ was found by taking the triple wedge integral as the sum of three single wedge integrals, and using the single wedge bounds derived by Werner [5] to find

$$\sup_{\rho} \left| \frac{1}{2} - \iint_{\Omega_3} dx dp W_{\rho}(x, p) \right| \leq 0.967\,820, \quad (20)$$

then using Eq. (13) to obtain the upper bound.

Now, we shall first present improved rigorous bounds of \mathbf{P}_3^{∞} , then use them to improve the bound for the negativity of the triple wedge. To start, we define the observable

$$\begin{aligned} A_3 &:= \left(Q_3^{\infty} - (1 - \mathbf{P}_3^c) \mathbb{1} \right) \left(Q_3^{\infty} - \mathbf{P}_3^c \mathbb{1} \right) \\ &= \left(Q_3^{\infty} - \frac{1}{2} \mathbb{1} \right)^2 - \left(\mathbf{P}_3^c - \frac{1}{2} \right)^2 \mathbb{1}, \end{aligned} \quad (21)$$

from which lower and upper bounds of $\text{maxeig}(A_3)$ can be rearranged into lower and upper bounds of \mathbf{P}_3^{∞} using $\text{maxeig}(A_3) = (\mathbf{P}_3^{\infty} - 1/2)^2 - (\mathbf{P}_3^c - 1/2)^2$.

The reason for working with A_3 instead of Q_3^{∞} is two-fold. First, the lower bound will be obtained by truncating the operator and finding its maximum eigenvalue, for

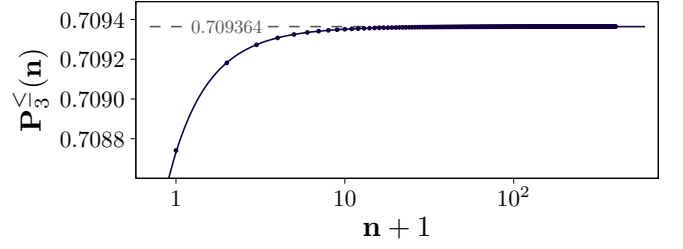


FIG. 4. Sequence of lower bounds $\mathbf{P}_3^{\leq}(\mathbf{n}) \leq \mathbf{P}_3^{\infty}$ against cutoff number \mathbf{n} , and numerical fit with the ansatz $\mathbf{P}_3^{\leq}(\mathbf{n}) = \mathbf{P}_3^{\infty} - a_1(\mathbf{n} + 1)^{-\frac{1}{2}} - a_2(\mathbf{n} + 1)^{-\frac{3}{2}} - \mathcal{O}[(\mathbf{n} + 1)^{-\frac{5}{2}}]$. The fitted parameters give $\mathbf{P}_3^{\infty} \approx 0.709\,364$, which corroborates the observation that $\lim_{\mathbf{n} \rightarrow \infty} \mathbf{P}_3^{\leq}(\mathbf{n}) = \mathbf{P}_3^{\infty} \approx 0.709\,364$.

which the sequence of lower bounds was found to converge faster with A_3 than with Q_3^{∞} . Second, the upper bound will be obtained from the trace of the observable, which requires removing the values \mathbf{P}_3^c and $1 - \mathbf{P}_3^c$ that are in the continuous spectra of Q_3^{∞} [2].

In Appendix A3, we derive an expression for the matrix elements of A_3 in the number basis $\{|n\rangle\}_{n=0}^{\infty}$, where $(X^2 + P^2)|n\rangle = (2n + 1)|n\rangle$. $\langle n|A_3|n'\rangle$ is given in terms of the incomplete beta function and the generalised hypergeometric function, which are commonly-used special functions that can be computed with standard numerical libraries to arbitrary precision.

The lower bound $\mathbf{P}_3^{\leq}(\mathbf{n}) \leq \mathbf{P}_3^{\infty}$ is then obtained by truncating A_3 to the subspace spanned by the first $6\mathbf{n} + 1$ number states $\{|n\rangle\}_{n=0}^{6\mathbf{n}}$ and solving for its maximum eigenvalue. $\mathbf{P}_3^{\leq}(\mathbf{n})$ is plotted against \mathbf{n} in Fig. 4. The largest lower bound we obtained is $\mathbf{P}_3^{\leq}(400) = 0.709\,364$: in fact, the sequence of lower bounds appears to saturate to this value, which would imply that $\lim_{\mathbf{n} \rightarrow \infty} \mathbf{P}_3^{\leq}(\mathbf{n}) = \mathbf{P}_3^{\infty} \approx 0.709\,364$. Furthermore, fitting the sequence of lower bounds to the ansatz $\mathbf{P}_3^{\leq}(\mathbf{n}) = \mathbf{P}_3^{\infty} - a_1(\mathbf{n} + 1)^{-\frac{1}{2}} - a_2(\mathbf{n} + 1)^{-\frac{3}{2}} - \mathcal{O}[(\mathbf{n} + 1)^{-\frac{5}{2}}]$ gives $\mathbf{P}_3^{\infty} \approx 0.709\,364$, which corroborates the observation.

Meanwhile, since $\Pi Q_3^{\infty} \Pi = \mathbb{1} - Q_3^{\infty}$ and $\Pi A_3^{\infty} \Pi = A_3^{\infty}$ for the parity operator Π that satisfies $\Pi X(\theta) \Pi = -X(\theta)$, every nonzero eigenvalue of A_3 is doubly degenerate. Therefore, an upper bound for \mathbf{P}_3^{∞} can be obtained using

$$\begin{aligned} \text{tr}(A_3^2) &= \frac{6 \log 2}{(18\pi)^2} \geq 2[\text{maxeig}(A_3)]^2 \\ &= 2 \left[\left(\mathbf{P}_3^{\infty} - \frac{1}{2} \right)^2 - \left(\mathbf{P}_3^c - \frac{1}{2} \right)^2 \right]^2. \end{aligned} \quad (22)$$

The analytical evaluation of the trace is given in Appendix A4. Relating this upper bound to \mathbf{P}_3^{∞} gives

$$\mathbf{P}_3^{\infty} \leq \frac{1}{2} \left(1 + \frac{1}{3} \sqrt{1 + \frac{2}{\pi} \sqrt{3 \log 2}} \right) \lesssim 0.730\,822. \quad (23)$$

In summary, we obtain rigorous lower and upper bounds

$$0.709\,364 \leq \mathbf{P}_3^\infty \leq 0.730\,822, \quad (24)$$

a stark improvement over Eq. (19). The sequence as plotted in Fig. 4 also strongly implies the tightness of the lower bound.

We finish by highlighting two consequences of the improved bounds. First, it is now rigorously proved that $\mathbf{P}_3^\infty < 3/4$, which is a value that can be achieved with suitable states of spin $j = 3/2$ and equally spaced angles (see Ref. [6] and Sec. IV). Thus, the score of the Tsirelson protocol is higher for finite-dimensional systems than for continuous variables. Second, using the new bounds, the bound of the triple wedge integral Eq. (18) becomes

$$0.628\,092 \leq \sup_\rho \left| \frac{1}{2} - \iint_{\Omega_3} dx dp W_\rho(x, p) \right| \leq 0.692\,464, \quad (25)$$

significantly tightening Eq. (20).

IV. SPIN ANGULAR MOMENTUM

The first generalisation of Tsirelson's original protocol extended it from phase space to real space by considering the precession of the angular momentum of a system [6]. A rotation of J_x by an angle θ around the $-z$ axis reads

$$J_x(\theta) = e^{-i\theta J_z} J_x e^{i\theta J_z} = J_x \cos \theta + J_y \sin \theta. \quad (26)$$

The observed score upon performing the precession protocol on $J_x(\theta)$ is $P(\vec{\theta}) = \text{tr}[\rho Q(\vec{\theta})]$, where

$$Q(\vec{\theta}) = \frac{1}{3} \sum_{k=0}^2 e^{-i\theta_k J_z} \Theta(J_x) e^{i\theta_k J_z}. \quad (27)$$

In terms of the simultaneous eigenstates $|j, m\rangle$ of $|\vec{J}|^2$ and J_z with eigenvalues $j(j+1)$ and m , respectively, the matrix elements of $Q(\vec{\theta})$ are known analytically, and it is also known that $Q(\vec{\theta}) = \bigoplus_j Q^{(j)}(\vec{\theta})$ can be decomposed into blocks with irreducible spin j [6]. As the score $P(\vec{\theta}) = \text{tr}[\rho Q(\vec{\theta})] = \sum_j \text{tr}[\rho Q^{(j)}(\vec{\theta})]$ is simply a sum of the expectation value on each $Q^{(j)}(\vec{\theta})$ block, we can restrict our analysis to the precession protocol performed for a fixed spin j .

For the rest of the paper, we shall denote the maximum quantum score for a fixed spin j as $\mathbf{P}^{(j)}(\vec{\theta}) := \max_\rho \text{tr}[\rho Q^{(j)}(\vec{\theta})]$, with analogous shorthands $Q_3^{(j)} := Q^{(j)}(\vec{\theta}_3)$ and $\mathbf{P}_3^{(j)} := \mathbf{P}^{(j)}(\vec{\theta}_3)$ for the original protocol.

A. Location of Local and Global Maxima

Unlike the harmonic oscillator case, no continuous symplectic transformations exist for the angular momentum operators, so the choice of probing angles affects

$\mathbf{P}^{(j)}(\vec{\theta})$, even in the interior region Δ where $\mathbf{P}^c(\vec{\theta}) = 2/3$. As such, it is of interest to find the choices of $\vec{\theta}$ that demonstrate large violations of the classical bound.

The maximum scores $\mathbf{P}^{(j)}(\vec{\theta})$, calculated with standard numerical tools to diagonalise the finite dimensional matrices $Q^{(j)}(\vec{\theta})$, are plotted against ϑ_1 and ϑ_2 as heatmaps for some select values of half integer spins in Fig. 5 and integer spins in Fig. 6.

A pattern becomes apparent by mere visual inspection. For the chosen sequences of spin, we find that there are a triangular number of local maxima, arranged exactly as per its definition as a figurate number. This pattern can be further appreciated by relating the symmetries of each spin particle with the symmetries of the protocol for the choices of angles.

For the equally-spaced protocol, it was previously understood that the large violation of $\mathbf{P}_3^{(3/2)} = 3/4$ by the cat state $\propto |3/2, 3/2\rangle - |3/2, -3/2\rangle$ came about because it was “*in resonance*” with the three probing times of the original protocol. That is, under a J_z rotation, states of a spin $j = 3/2$ particle can only have discrete symmetries of integer multiples of $2\pi/(2j) = 2\pi/3$ rotations. Since the original protocol respects exactly this symmetry, a large quantum score can be achieved by preparing a state with that symmetry that has a large initial component of $\Theta(J_x)$. This intuition was validated by plotting the spherical Wigner function of the maximally-violating state in Fig. 7, where it can be clearly seen that the score is augmented by the constructive interference that occurs at angles that are $2\pi/3$ apart.

Now, if we compare this to the Wigner function of maximally-violating states at the local peaks for other choices of j , as with the spin-7/2 and spin-5 cases plotted in Fig. 8, we observe again that the constructive interference occurs at angles that are about $2\pi/(2j)$ apart. As such, the choices of $\vec{\theta}$ must be such that the probing angles satisfy $\theta_k \approx n_k 2\pi/(2j)$ for integers n_k . Together with Eq. (5) and $\theta_1 \leq \theta_2$, this gives the “*resonant angles*”

$$\vec{\theta}_\Delta^{(j)}(n_1, n_2) := \left(\frac{n_1\pi}{j}, \frac{n_2\pi}{j} \right) \quad (28)$$

where n_1 and n_2 are integers such that $1 \leq n_1 \leq \lfloor j-1/2 \rfloor$ and $1 + \lfloor j \rfloor \leq n_2 \leq n_1 + \lfloor j-1/2 \rfloor$. For a given j , the number of points at which the condition is satisfied at is

$$\sum_{n_1=1}^{\lfloor j-\frac{1}{2} \rfloor} \sum_{n_2=1+\lfloor j \rfloor}^{n_1+\lfloor j-\frac{1}{2} \rfloor} = \left\lfloor j - \frac{1}{2} \right\rfloor \left(\frac{1}{2} + \frac{3}{2} \left\lfloor j - \frac{1}{2} \right\rfloor - \lfloor j \rfloor \right), \quad (29)$$

which for the sequences $j = 3/2, 5/2, 7/2, 9/2, \dots$ for the half integer spins and $j = 3, 4, 5, 6, \dots$ for the integer spins, give exactly the sequence of triangular numbers $1, 3, 6, 10, \dots$.

Looking back to the protocol scores in Figs. 5 and 6, the local maxima are indeed found in the vicinity of, although not always exactly at, the resonant angles. Among those local maxima, the global maxima are found

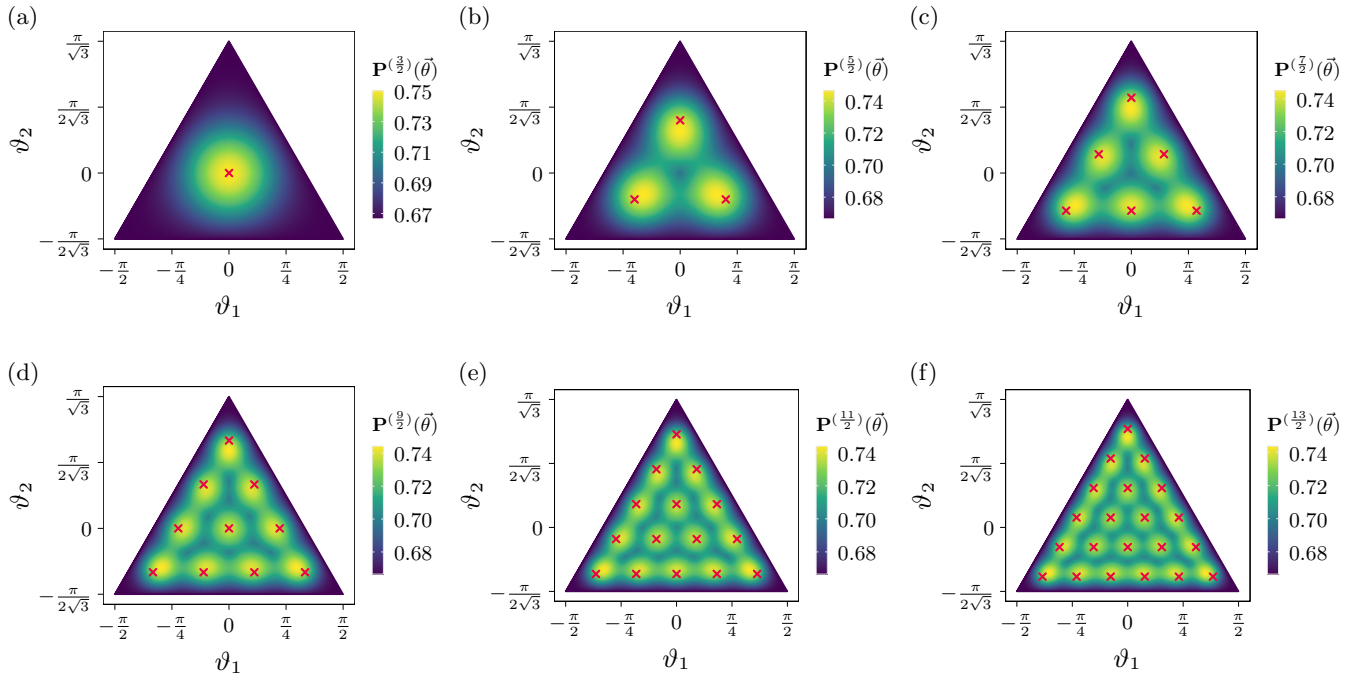


FIG. 5. Heatmaps of $\mathbf{P}^{(j)}(\vec{\theta})$ for half-integer spins (a) $j = 3/2$, (b) $j = 5/2$, (c) $j = 7/2$, (d) $j = 9/2$, (e) $j = 11/2$, (f) $j = 13/2$, plotted in the $\vec{\theta}$ coordinates. Notice that the local peaks follow the triangle numbers $1, 3, 6, 10, \dots$. The resonant angles $\vec{\theta}_{\Delta}^{(j)}(n_1, n_2) = \frac{2\pi}{2j}(n_1, n_2)$ for integers n_1 and n_2 are also crossed out in red.

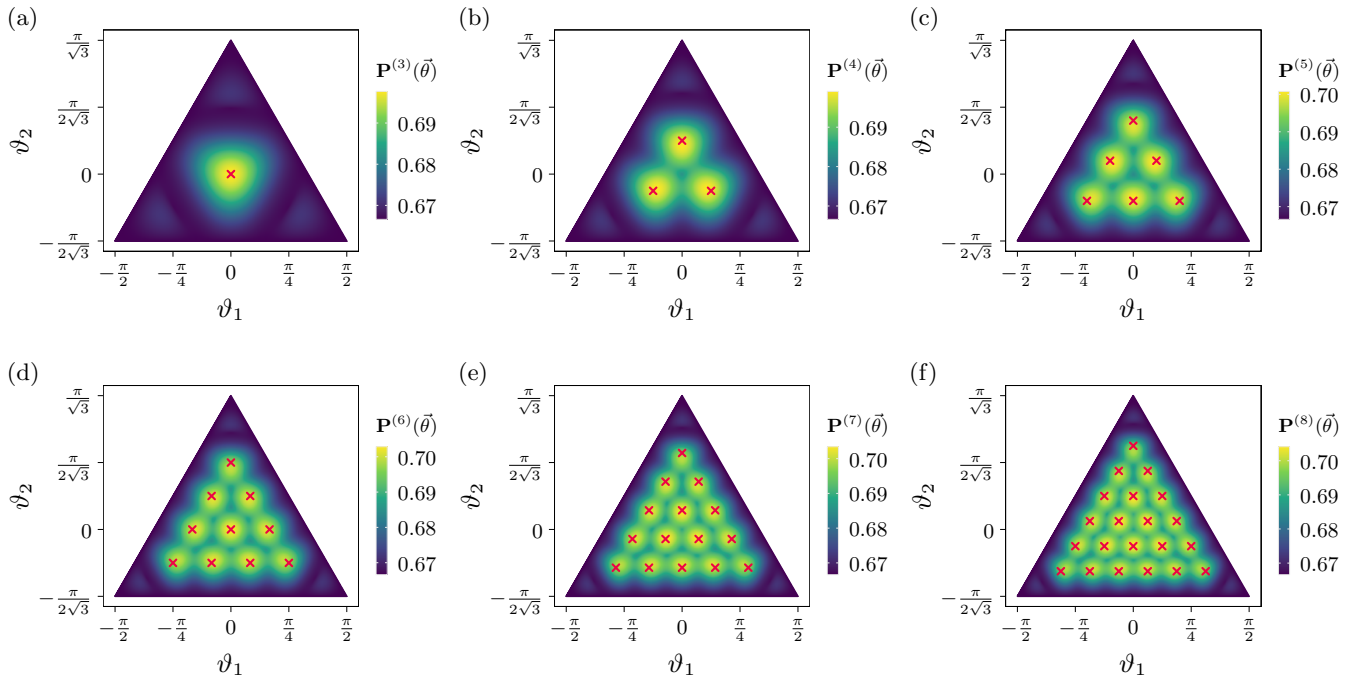


FIG. 6. Heatmaps of $\mathbf{P}^{(j)}(\vec{\theta})$ for integer spins (a) $j = 3$, (b) $j = 4$, (c) $j = 5$, (d) $j = 6$, (e) $j = 7$, (f) $j = 8$, plotted in the $\vec{\theta}$ coordinates. As with Fig. 5, the local peaks follow the triangle numbers, and the resonant angles $\vec{\theta}_{\Delta}^{(j)}$ are crossed out in red.

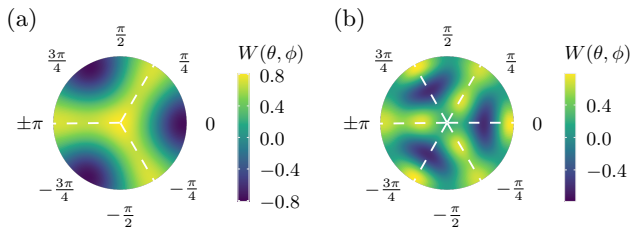


FIG. 7. Stereoscopic projection of the $J_z \geq 0$ hemisphere of the spherical Wigner function $W(\theta, \phi)$ [20] of the states that achieve the maximum scores (a) $\mathbf{P}_3^{(3/2)} = 3/4$ for a spin-3/2 particle and (b) $\mathbf{P}_3^{(3)} = (8 + \sqrt{10})/16 \approx 0.698$ for a spin-3 particle. The constructive interferences that occur at angles that are $2\pi/3$ apart for spin-3/2 and $\pi/3$ apart for spin-3 augment the scores to enable large violations of the classical bound.

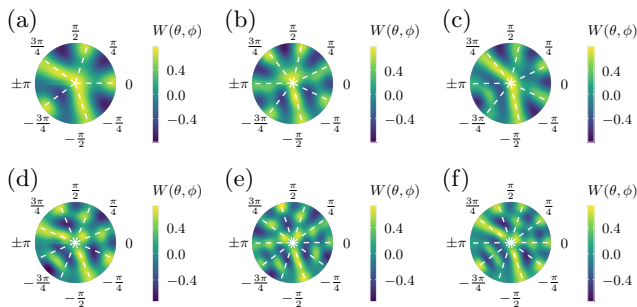


FIG. 8. Wigner function of the states that achieve the local peaks in Fig. 5 of the (a) spin-5/2, (b,c) spin-7/2, (d) spin-4, and (e,f) spin-5 particles. The constructive interferences occur at angles that are $2\pi/2j$ apart, similarly to the spin-3/2 case in Fig. 7, although the interference patterns are far more complicated.

close to $\vec{\theta}_\Delta^{(j)}(n_G, 2n_G)$ by inspection, and the equivalent choices with respect to the symmetry in Eq. (6), where

$$n_G = \begin{cases} \lfloor (2j+1)/3 \rfloor & \text{for } j \text{ integer,} \\ \lfloor j \rfloor & \text{for } j \text{ half-integer.} \end{cases} \quad (30)$$

With these observation, we can try to find an even better approximation of the local maxima than the resonant angles. In Appendix A5, we use the latter as initial points in the gradient descent optimisation of $\mathbf{P}^{(j)}(\vec{\theta})$. There, we heuristically found the local maxima to occur at $\vec{\theta}_\Delta^{(j)} \approx \lambda_j \vec{\theta}_\Delta^{(j)} + (1 - \lambda_j) \vec{\theta}_3$, where

$$\frac{1}{\lambda_j} = 1 + \begin{cases} \frac{0.533051}{j-0.213570} & \text{for } j \text{ integer,} \\ \frac{0.554086}{j-0.197425} & \text{for } j \text{ half-integer.} \end{cases} \quad (31)$$

In other words, the optimal probing angles are approximately the convex combination of the probing angles that reflect the discrete symmetries of the spin system ($\vec{\theta}_\Delta^{(j)}$)

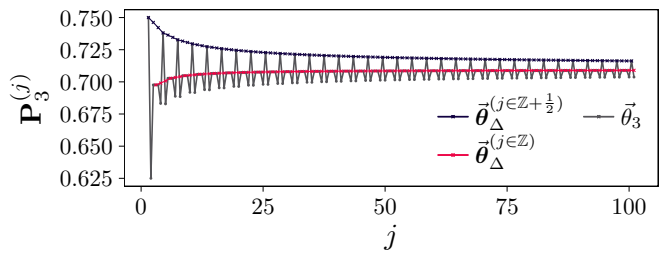


FIG. 9. The scores $\mathbf{P}_3^{(j)}$ of the original equally-spaced precession protocol against j , superimposed with $\mathbf{P}^{(j)}[\vec{\theta}^{(j)}(n_0, 2n_0)]$, where $(n_0, 2n_0)$ is the local peak closest to $\vec{\theta}_3$.

and those that reflect the discrete symmetries of the protocol ($\vec{\theta}_3$). While our approximate expressions for $\vec{\theta}_\Delta^{(j)}$ are heuristic, they may come in handy as approximate values to choose in an experiment, or as starting points for even more precise optimisations.

B. Behaviour of $\mathbf{P}^{(j)}(\vec{\theta})$ against j

We are now able to revisit some properties of the obtained scores, referring to Fig. 9. In Ref. [6], we had already plotted $\mathbf{P}_3^{(j)}$ against j and observed a damped oscillatory pattern. The damping behaviour was explained by proving analytically that $\lim_{j \rightarrow \infty} \mathbf{P}_3^{(j)} = \mathbf{P}_3^\infty$, but an explanation for the oscillatory behaviour eluded us. With our new understanding of the location of the local maxima, we see that the oscillatory behaviour came from the fact that the probing angles $\vec{\theta}_3$ of original protocol only corresponds to a resonant angle $\vec{\theta}_\Delta^{(j)}$ when $2j$ is a multiple of three. In the other cases, $\vec{\theta}_3$ lies in between three peaks and is in fact a local minimum.

If we now adapt the angles and plot the local maxima obtained by gradient descent with the initial point at the origin, equivalently given by $\vec{\theta}_\Delta(n_0, 2n_0)$ with $n_0 = \lfloor (2j+1)/3 \rfloor$, we find that the score as a function of j plots two different smooth sequences, one for half-integer spins and the other for integer spins. Both sequences converge towards \mathbf{P}_3^∞ . More generally, we observe in Fig. 10 that every point in the interior of Δ approaches \mathbf{P}_3^∞ for large spins, which is due to the convergence $Q^{(j)}(\vec{\theta}) \rightarrow Q^\infty(\vec{\theta})$ as $j \rightarrow \infty$ for any fixed $\vec{\theta}$ [6].

C. Improved Conjectured Bounds of \mathbf{P}_3^∞

Due to the convergence $\lim_{j \rightarrow \infty} \mathbf{P}^{(j)}(\vec{\theta}) = \mathbf{P}_3^\infty$, every value $\mathbf{P}^{(j)}(\vec{\theta})$ for sufficiently large j is an approximation for \mathbf{P}_3^∞ . Furthermore, we observe that the sequence of $\mathbf{P}^\infty[\vec{\theta}_\Delta^{(j)}(n_0, 2n_0)]$ for integer j (respectively, half-integer j) in Fig. 9 seem to be monotonically increasing (respectively, monotonically decreasing). We conjecture that

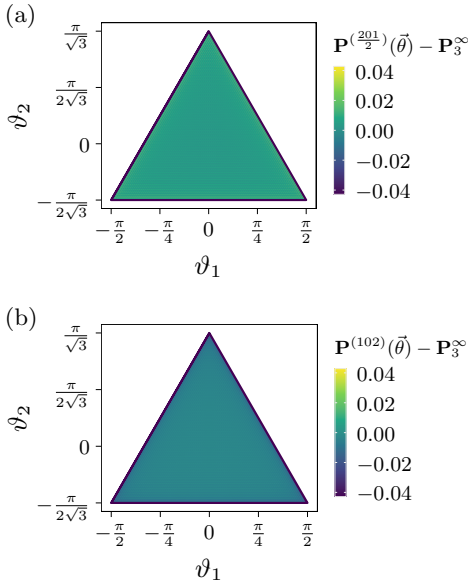


FIG. 10. Heatmap of $\mathbf{P}_3^{(j)}(\vec{\theta}) - 0.709364$, where $\mathbf{P}_3^\infty \approx 0.709364$ is the approximate value of the maximum score of the quantum harmonic oscillator. The scores $\mathbf{P}_3^{(j)}(\vec{\theta})$ in the interior of the half-integer spin (integer spin) are all slightly larger (slightly smaller) than but close to \mathbf{P}_3^∞ .

this is indeed the case:

Conjecture. *We conjecture that the integer (half-integer) subsequence of $\mathbf{P}_3^{(3n/2)}$ is monotonically increasing (decreasing) in n , that is,*

$$n \leq n' \implies \begin{cases} \mathbf{P}_3^{((2n)3/2)} \leq \mathbf{P}_3^{((2n')3/2)}, \\ \mathbf{P}_3^{((2n+1)3/2)} \geq \mathbf{P}_3^{((2n'+1)3/2)}. \end{cases} \quad (32)$$

Note that we focus on the subsequence where j is a multiple of $3/2$ as $\mathbf{P}_3^{(3n/2)}[\vec{\theta}_\Delta(n_0, 2n_0)] = \mathbf{P}_3^{(3n/2)}$ can be more easily computed for large n as $Q_3^{(3n/2)}$ is block-diagonal in that case [6].

We checked that this conjecture is true for the first 5500 terms of both subsequences, as shown in Fig. 11. If this conjecture holds for the for all j , combined with the fact that both sequences approach \mathbf{P}_3^∞ , this means that $\mathbf{P}_3^{((2n)3/2)} \leq \mathbf{P}_3^\infty \leq \mathbf{P}_3^{((2n'+1)3/2)}$ for any $n, n' \geq 0$. This provides us with conjectured bounds $\mathbf{P}_3^{(225000)} = 0.709364 \leq \mathbf{P}_3^\infty \leq 0.709511 = \mathbf{P}_3^{(390003/2)}$ for the maximum score of the quantum harmonic oscillator.

Furthermore, we fitted both subsequences with the asymptotic ansatz

$$\mathbf{P}_3^{(j=3n/2)} = \begin{cases} \mathbf{P}_3^\infty - \sum_{l=1}^2 b_l j^{-l} + \mathcal{O}(j^{-3}) & \text{for } n \text{ even,} \\ \mathbf{P}_3^\infty + \sum_{l=1}^4 c_l j^{-\frac{l}{2}} + \mathcal{O}(j^{-\frac{5}{2}}) & \text{otherwise,} \end{cases} \quad (33)$$

which is also plotted in Fig. 11. For both numerical fits, the fitted parameters were in agreement with the numerical fit of $\mathbf{P}_3^\infty = 0.709364$ of the rigorous lower bound

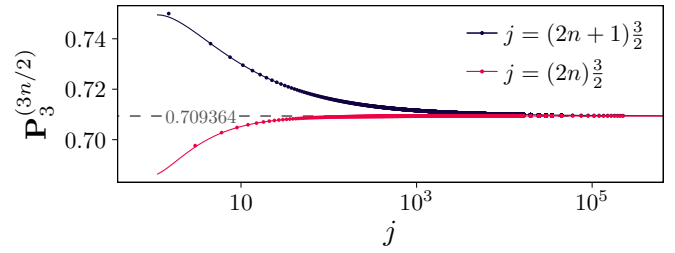


FIG. 11. The score $\mathbf{P}_3^{(j)}$ when $2j$ is a multiple of 3. We conjecture that $\mathbf{P}_3^{(3n/2)}$ is monotonically increasing (decreasing) for n even (n odd), so their convergence to \mathbf{P}_3^∞ would imply that their values for n even (n odd) form a sequence of lower bounds (upper bounds) of \mathbf{P}_3^∞ . We also perform a numerical fit to the ansatz given in Eq. (33), which implies that both sequences converge to $\lim_{n \rightarrow \infty} \mathbf{P}_3^{(3n/2)} = \mathbf{P}_3^\infty = 0.709364$.

in Fig. 4 to twelve decimal places. All in all, the numerical evidence strongly suggests that the true value of the maximum score of the quantum harmonic oscillator is indeed $\mathbf{P}_3^\infty = 0.709364$.

V. IMPLICATIONS ON DETECTING ENTANGLEMENT

The original precession protocol has been shown to be useful for detecting entanglement when performed on a collective coordinate of the system. In this section, we show how these previous results carry over to generalisations of the precession protocol.

A. Witnessing Non-Gaussian Entanglement of Coupled Harmonic Oscillators

Reference [9] considered two coupled harmonic oscillators, with local coordinates (X_n, P_n) for the n th oscillator, of the form

$$\begin{aligned} H &= \sum_{n=1}^2 \frac{\omega_n}{2} (X_n^2 + P_n^2) - \frac{g}{2} X_1 X_2 \\ &= \sum_{\sigma \in \{+, -\}} \frac{\omega_\sigma}{2} (X_{\sigma\varphi}^2 + P_{\sigma\varphi}^2), \end{aligned} \quad (34)$$

with collective coordinates $X_{+\varphi} = X_1 \cos \varphi + X_2 \sin \varphi$ and $X_{-\varphi} = X_2 \cos \varphi - X_1 \sin \varphi$, similarly defined for $P_{\pm\varphi}$, where $\varphi = \arctan(g, \omega_1^2 - \omega_2^2)$. By performing the precession protocol on the collective coordinate $X_{\sigma\varphi}(t)$ for $\sigma \in \{+, -\}$, entanglement between the local coordinates can be detected when the obtained score $P_{3,\sigma}^\infty(\varphi) := \text{tr}[\rho Q_{3,\sigma}^\infty(\varphi)]$, where $3Q_{3,\sigma}^\infty(\varphi) := \sum_{k=0}^2 \Theta[X_{\sigma\varphi}(2\pi k/3\omega_\sigma)]$, satisfies

$$P_{3,\sigma}^\infty(\varphi) > \mathbf{P}_3^{\infty\text{-sep}}(\varphi) := \max_{\varrho: \varrho^{T_2} \geq 0} \text{tr}[\varrho Q_{3,\sigma}^\infty(\varphi)]. \quad (35)$$

Here, ρ^{T_2} is the partial transpose over the (X_2, P_2) mode. The special case $\mathbf{P}_3^{\infty\text{-sep}}(\pi/4) = \mathbf{P}_3^c$ is known analytically due to the relationship between Wigner negativity and entanglement [9, 21] (see in particular Theorem 2 of Ref. [22]), while the general case can be calculated using semidefinite programming by truncating the energy levels [9].

The same idea can be applied to the family of precession protocols with three angles. For a choice of probing time $\vec{\theta}$, we can similarly perform the protocol on the collective coordinate $X_{\sigma\varphi}(t)$ to obtain the score $P_\sigma^\infty(\varphi, \vec{\theta}) := \text{tr}[\rho Q_\sigma^\infty(\varphi, \vec{\theta})]$, where $3Q_\sigma^\infty(\varphi, \vec{\theta}) := \sum_{k=0}^2 \Theta[X_{\sigma\varphi}(\theta_k/\omega_\sigma)]$. Then, entanglement is detected when $P_\sigma^\infty(\varphi, \vec{\theta}) > \mathbf{P}^{\infty\text{-sep}}(\varphi, \vec{\theta})$, where the separable bound is similarly defined as

$$\mathbf{P}^{\infty\text{-sep}}(\varphi, \vec{\theta}) := \max_{\varrho: \varrho^{T_2} \succeq 0} \text{tr} \left[\varrho Q_\sigma^\infty(\varphi, \vec{\theta}) \right]. \quad (36)$$

In Appendix A6, we show that for all points in the interior region Δ such that $\mathbf{P}^c(\vec{\theta}) = 2/3$, we have $\mathbf{P}^{\infty\text{-sep}}(\varphi, \vec{\theta}) = \mathbf{P}_3^{\infty\text{-sep}}(\varphi)$. This means that the separable bounds previously found in Ref. [9] also hold for all three angle precession protocols performed on a collective mode. In particular, $\mathbf{P}^{\infty\text{-sep}}(\pi/4, \vec{\theta}) = \mathbf{P}_3^c$ for all $\vec{\theta}$ in the interior.

These results allow us to witness the non-Gaussian entanglement of states that could not be detected with the original protocol. For example, consider the state

$$\begin{aligned} |\chi_4\rangle = & \frac{1}{\sqrt{10}} \left[2 \cos(10/17) |0\rangle_+ - \sqrt{5} \sin(2/3) |1\rangle_+ \right. \\ & + 2 \sin(10/17) |2\rangle_+ - \sqrt{5} \cos(2/3) |3\rangle_+ \\ & \left. + |4\rangle_+ \right] \otimes |0\rangle_-, \end{aligned} \quad (37)$$

where $|n\rangle_\pm$ are the number states in the collective mode $(X_{\pm\pi/4}, P_{\pm\pi/4})$. $|\chi_4\rangle$ does not violate the original protocol as there are no states truncated to the first five energy levels for which $P_3^\infty > \mathbf{P}_3^c$ [11]. However, $P_\sigma^\infty[\pi/4, (\pi^2/4, \pi^2/2)] = 0.669 > \mathbf{P}_3^c$ when performed on the collective mode $X_{+\pi/4}$, so we can detect the entanglement of $|\chi_4\rangle$ with a different set of probing angles.

Another important application is to relate the detection of squeezed versions of states. Recently, advances in bosonic error correction has led to the development of squeezed cat codes of the form $\propto \sum_{k=0}^{K-1} S_\lambda |\alpha e^{i\frac{2\pi k}{K}}\rangle$ where $S_\lambda := \exp[-i\lambda(XP + PX)/2]$ is the squeeze operator, which is robust against a variety of error sources [23, 24]. Previously, it was found that the entanglement of the entangled tricat state $|\text{cat}_3(\alpha)\rangle \propto \sum_{k=0}^2 |\alpha e^{i\frac{2\pi k}{3}}\rangle \otimes |\alpha e^{i\frac{2\pi k}{3}}\rangle$ could be detected with the original precession protocol for certain values of α for which $P_{3,+}^\infty(\pi/4) > \mathbf{P}_3^c$ [9]. From the relation $S_\lambda^{\otimes 2} Q_{3,+}^\infty(\pi/4) S_\lambda^{\dagger \otimes 2} = Q_+^\infty[\pi/4, (\tilde{\theta}_-, \tilde{\theta}_+)]$ that comes from the constructive proof of Theorem A3, where $\tilde{\theta}_\mp = \pi \mp \text{atan}(\sqrt{3}e^{2\lambda})$, the squeezed version of the cat state

$S_\lambda^{\otimes 2} |\text{cat}_3(\alpha)\rangle$ can be detected by performing the precession protocol on a collective mode with probing angles $\vec{\theta} = (\tilde{\theta}_-, \tilde{\theta}_+)$, since

$$\begin{aligned} & P_+^\infty[\pi/4, (\tilde{\theta}_-, \tilde{\theta}_+)] \\ &= \langle \text{cat}_3(\alpha) | S_\lambda^{\dagger \otimes 2} Q_+^\infty[\pi/4, (\tilde{\theta}_-, \tilde{\theta}_+)] S_\lambda^{\otimes 2} | \text{cat}_3(\alpha) \rangle \\ &= \langle \text{cat}_3(\alpha) | Q_{3,+}^\infty(\pi/4) | \text{cat}_3(\alpha) \rangle \\ &= P_{3,+}^\infty(\pi/4) > \mathbf{P}_3^c. \end{aligned} \quad (38)$$

B. Witnessing Genuine Multipartite Entanglement with Collective Spin Measurements

Reference [10] considered ensembles of N particles with fixed spins $\{j_n\}_{n=1}^N$, where j_n is the spin of the n th particle. There, it was shown that for any observable defined by a function $f(\vec{J})$ of the total angular momentum $\vec{J} = \sum_{n=1}^N \vec{J}^{(j_n)}$ of the system,

$$\begin{aligned} \text{tr} \left[\rho f(\vec{J}) \right] &> \max_{j+j' \leq \sum_{n=1}^N j_n} \max_{\varrho \in \text{PPT}_{j,j'}} \text{tr} \left[\varrho f(\vec{J}^{(j)} + \vec{J}^{(j')}) \right] \\ &\implies \rho \text{ is genuinely multipartite entangled,} \end{aligned} \quad (39)$$

where $\text{PPT}_{j,j'}$ is the set of positive partial transpose states over the tensor product of a spin- j and spin- j' system. Here, ρ being genuinely multipartite entangled (GME) means that ρ is not a probabilistic mixture of states separable over any bipartition of the N spins.

One can then perform the precession protocol on the total angular momentum of the spin ensemble with any choice of probing angles, for which the score will be given by $P(\vec{\theta}) := \text{tr}[\rho Q^{\{\{j_n\}_n\}}(\vec{\theta})]$ where $3Q^{\{\{j_n\}_n\}}(\vec{\theta}) := \sum_{k=0}^n \Theta[(\cos \theta_k, \sin \theta_k, 0) \cdot \vec{J}]$. Since $Q^{\{\{j_n\}_n\}}(\vec{\theta})$ is a function of the total angular momentum, we can define the separable bound as

$$\mathbf{P}^{\text{sep}}(\{j_n\}_{n=1}^N, \vec{\theta}) := \max_{j,j' \leq \sum_n j_n} \underbrace{\max_{\varrho \in \text{PPT}_{j,j'}} \text{tr} \left[\varrho Q^{\{\{j,j'\}}(\vec{\theta}) \right]}_{\mathbf{P}^{\text{sep}}(\{j,j'\}, \vec{\theta})}, \quad (40)$$

which can be written as a maximisation over biseparable bounds $\mathbf{P}^{\text{sep}}(\{j,j'\}, \vec{\theta})$. This can in turn be calculated using semidefinite programming, whose results are shown in Fig. 12. We found that $\mathbf{P}^{\text{sep}}(\{j_n\}_{n=1}^N, \vec{\theta}) \leq \mathbf{P}_3^c$ when $\sum_n j_n \leq 2$. Hence, whenever a spin ensemble with total spin ≤ 2 violates the classical bound, its constituents must be GME.

We are also able to detect more states with this larger family of GME witnesses. For example, consider the state $e^{-i(49\pi/60)J_z} |\psi_4\rangle$ of a four-particle ensemble of spin-1/2 particles, where

$$\begin{aligned} |\psi_4\rangle = & \frac{\sqrt{6}+1}{6} |\Phi_+\rangle^{\otimes 2} + \frac{\sqrt{6}-1}{6} |\Phi_-\rangle^{\otimes 2} + \frac{1}{3} |\Psi_+\rangle^{\otimes 2} \\ & + \frac{1}{2} (|\Phi_+\rangle \otimes |\Psi_+\rangle + |\Psi_+\rangle \otimes |\Phi_+\rangle), \end{aligned} \quad (41)$$

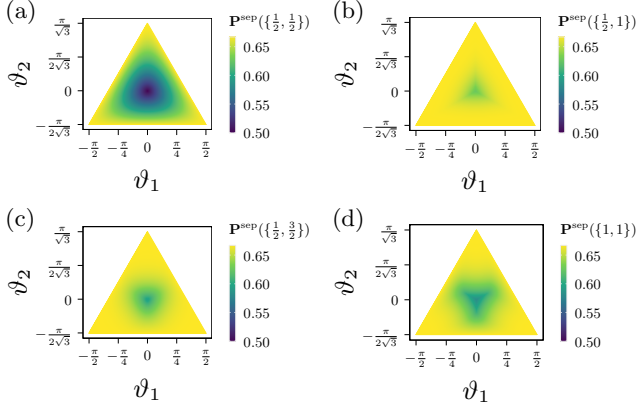


FIG. 12. Biseparable bounds $\mathbf{P}^{\text{sep}}(\{j, j'\}, \vec{\theta})$ for (a) $\{j, j'\} = \{1/2, 1/2\}$, (b) $\{j, j'\} = \{1/2, 1\}$, (c) $\{j, j'\} = \{1/2, 3/2\}$, and (d) $\{j, j'\} = \{1, 1\}$. For $j + j' \leq 2$, we find that the biseparable bounds satisfy $\mathbf{P}^{\text{sep}}(\{j, j'\}, \vec{\theta}) \leq \mathbf{P}_3^c$. As such, $\mathbf{P}^{\text{sep}}(\{j_n\}_n, \vec{\theta}) \leq \mathbf{P}_3^c$ for $\sum_n j_n \leq 2$, so GME is implied when the classical bound is violated upon performing any of the three-angle generalised precession protocols on the total angular momentum of a system with total spin at most two.

such that $|\Psi_{\pm}\rangle \propto |\uparrow\downarrow\rangle \pm |\downarrow\uparrow\rangle$ and $|\Phi_{\pm}\rangle \propto |\uparrow\uparrow\rangle \pm |\downarrow\downarrow\rangle$ are the Bell states. This state achieves the score $P_3 = 0.6 < \mathbf{P}_3^c$ for the original protocol performed on the total angular momentum, and the score $P(49\pi/60, 49\pi/30) = 0.67 > \mathbf{P}_3^c$ for the modified protocol. Therefore, the GME of $e^{-i(49\pi/60)J_z} |\psi_4\rangle$ can only be detected by the modified protocol and not the original one.

VI. IMPLICATIONS AND OUTLOOK ON PROTOCOLS WITH MORE ANGLES

In Ref. [6], the precession protocol was generalised to K equally-spaced angles for odd K —note that there is also a related protocol for even K [25], but it is rather different and not discussed in this paper. Just like the preceding sections, we consider now the generalisation to K arbitrarily-spaced angles. The K measured angles can be labelled such that $0 = \theta_0 \leq \theta_1 \leq \dots \leq \theta_{K-1} \leq 2\pi$, again up to an offset, so a particular choice of probing angles is specified by the vector $\vec{\theta} := (\theta_k)_{k=1}^{K-1}$.

In Appendix A1, we show that $\mathbf{P}^c(\vec{\theta}) = 1 - \delta/K$ for $\delta \in \{0, 1, \dots, (K-1)/2\}$ if and only if

$$\forall k : \theta_{(k \oplus_K \delta)} \ominus_{2\pi} \theta_k \leq \pi, \quad (42)$$

with a reminder that $x \oplus_m y = (x \pm y) \bmod m$ are addition and subtraction modulo m , respectively. The parameter space $\vec{\theta}$ is therefore split into $(K+1)/2$ regions where $\mathbf{P}^c \in \{1 - \delta/K\}_{\delta=0}^{(K-1)/2}$. For $K = 3$, these are precisely triangular regions with $\mathbf{P}^c = 2/3$ and $\mathbf{P}^c = 1$, respectively, but the regions become more complex to characterise for $K > 3$.

A. Quantum Harmonic Oscillator

For the $K = 3$ case, the scores in the interior region Δ are all $\mathbf{P}^{\infty}(\vec{\theta}) = \mathbf{P}_3^{\infty}$ because every observable $Q^{\infty}(\vec{\theta})$ within the same region can be symplectically transformed to each other. However, because there are only three degrees of freedom—change of phase, magnitude of squeezing, axis of squeezing—once 3 out of the K angles are transformed, the other $K - 3$ angles are fixed. Therefore, for $K > 3$ the different observables $Q^{\infty}(\vec{\theta})$ within the same region are no longer symplectically related, and so the maximum quantum score $\mathbf{P}^{\infty}(\vec{\theta})$ is no longer the same within the region with the same classical score.

Meanwhile, the upper bound $\mathbf{P}^{\geq}(\vec{\theta}) \geq \mathbf{P}^{\infty}(\vec{\theta})$ within the region where $\mathbf{P}^c(\vec{\theta}) = (1 + 1/K)/2$ can be found by extending the derivation of the upper bound \mathbf{P}_3^{\geq} . In principle, closed-form expressions of $\mathbf{P}^{\geq}(\vec{\theta})$ can be obtained, and the steps required to do so are laid out in Appendix A7. However, the obtained expressions are extremely cumbersome for $K > 3$, so we have instead evaluated $\mathbf{P}^{\geq}(\vec{\theta})$ numerically. This only involved integrals over piecewise smooth function, and thus the calculated bounds, although obtained numerically, are reliable.

In Fig. 13, we plot the upper bound \mathbf{P}_K^{\geq} of the maximum quantum score \mathbf{P}_K^{∞} for the equally-spaced protocol $\vec{\theta}_K := (2\pi k/K)_{k=1}^{K-1}$. The best upper bound previously known was $\mathbf{P}_K^{\infty} \leq \mathbf{P}_K^{\geq \text{old}} = \mathbf{P}_K^c + 0.155940$, which again came from bounds of the single-wedge integral of Wigner functions. However, $\mathbf{P}_K^{\geq \text{old}}$ saturates at $1/2 + 0.155940$ as $K \rightarrow \infty$, which is the incorrect asymptotic behaviour, as it is known that $\lim_{K \rightarrow \infty} \mathbf{P}_K^{\infty} = 1/2$ [6]. Rather, the new upper bound \mathbf{P}_K^{\geq} not only exhibits the correct asymptotic behaviour, but is also close to the previously-known lower bound \mathbf{P}_K^{\leq} [6]. Furthermore, the new upper bound in turn provides an improved upper bound of

$$\sup_{\rho} \left| \frac{1}{2} - \iint_{\Omega_K} dx dp W_{\rho}(x, p) \right| \leq K \left(\mathbf{P}_K^{\geq} - \frac{1}{2} \right), \quad (43)$$

where $\Omega_K = \{(x, p) : \text{atan}(p, x) \bmod (4\pi/K) \leq 2\pi/K\}$ is the equally-spaced K -wedge region.

B. Spin Angular Momentum

Lastly, we consider the precession protocol with more probing angles applied to spin angular momentum. While we can no longer plot out $\mathbf{P}^{(j)}(\vec{\theta})$ for the full parameter space like we did for $K = 3$, we can try to observe some properties of the local peaks by starting with random initial parameters $\vec{\theta}$ and performing gradient descent. We observe that some qualitative behaviour carries over from the $K = 3$ case. For example, for $K = 5$, we notice that many local peaks occur for $\vec{\theta}_{\Delta}^{(j)} \approx \vec{\theta}_{\lambda}^{(j)} := (1 - \lambda)\vec{\theta}_{\Delta}^{(j)} + \lambda\vec{\theta}_K$ region, where

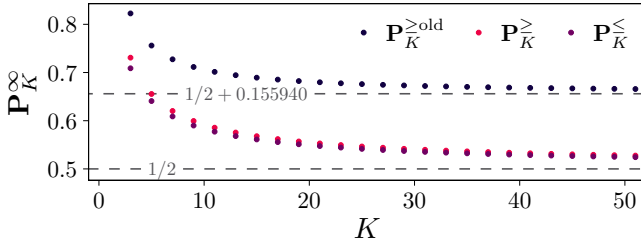


FIG. 13. Plot of the upper bound $\mathbf{P}_K^{\geq} \geq \mathbf{P}_K^{\infty}$ for the quantum harmonic oscillator, and for the equally-spaced protocol; with comparison to the previously known bounds from Ref. [6], lower \mathbf{P}_K^{\leq} and upper $\mathbf{P}_K^{\geq \text{old}} = \mathbf{P}_K^e + 0.155940$. The improved upper bound exhibits the correct asymptotic behaviour for $\lim_{K \rightarrow \infty} \mathbf{P}_K^{\infty} = 1/2$, and is also very close to \mathbf{P}_K^{\leq} .

$\vec{\theta}_{\Delta}^{(j)} = (\pi n_k/j)_{k=1}^{K-1}$, and $\{n_k\}_{k=1}^{K-1}$ are integers such that

$$0 < n_1 < \dots < n_{\frac{K-1}{2}} \leq [j] < n_{\frac{K+1}{2}} < \dots \leq K-1. \quad (44)$$

This is shown in Fig. 14 for $j \in \{7/2, 11/2\}$, where we plot the distance between $\vec{\theta}$ and the closest mixture $\vec{\theta}_{\lambda}^{(j)}$ as we increase the number of iterations of the gradient descent algorithm. Many initial points converge to $\vec{\theta}_{\lambda}^{(j)}$, which shows that they are still local maxima even in the $K = 5$ case. However, we also observe local maxima that are not of the form $(1-\lambda)\vec{\theta}_{\Delta}^{(j)} + \lambda\vec{\theta}_K$. That said, this observation helps us choose good initial points for performing the gradient descent. In Fig. 15, we contrast random initial points with initial points of the form $(\vec{\theta}_{\Delta}^{(j)} + \vec{\theta}_K)/2$. We find that the chosen initial points already start with large violations, and converge much faster to the local maximum than randomly chosen parameters. This aids in finding states and parameters $\vec{\theta}$ that obtain large scores $\mathbf{P}^{(j)}(\vec{\theta})$, similar to those prepared in recent experimental implementations of the precession protocol [8].

VII. CONCLUSION

In this work, we have characterised the family of Tsirelson's precession protocol with three angles, which include as special cases some previously-studied generalisations like the Type I and II Tsirelson inequalities. We answer an open question about the maximum violation possible for these inequalities by showing that the maximum score for the harmonic oscillator is the same for all members of the characterised family. Furthermore, we provide new rigorous and conjectured bounds for the maximum quantum score \mathbf{P}_3^{∞} of the original protocol that improve upon the best bounds that were previously known, which also contribute improved bounds of integrals of Wigner functions over certain phase space regions. Finally, by extrapolating the rigorous and conjectured bounds, we estimate that the true value of the maximum quantum score is $\mathbf{P}_3^{\infty} = 0.709364$.

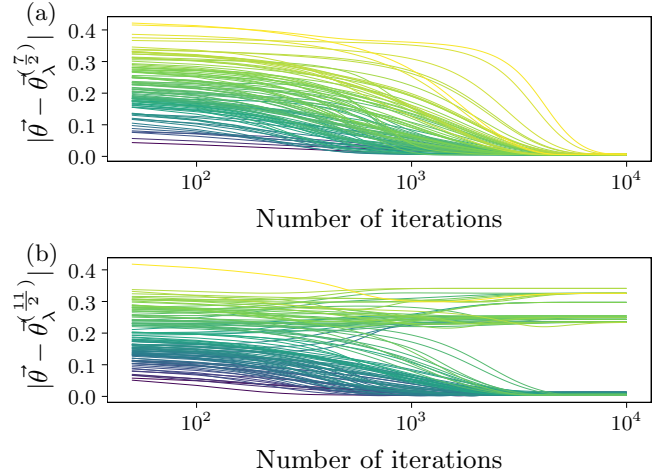


FIG. 14. Distance of probing angles $\vec{\theta}$ to closest mixture $\vec{\theta}_{\lambda}^{(j)} = (1-\lambda)\vec{\theta}_{\Delta}^{(j)} + \lambda\vec{\theta}_K$ against the number of iterations of the gradient descent, with $K = 5$, for (a) $j = 7/2$ and (b) $j = 11/2$. The location of many local peaks are close to $\vec{\theta}_{\lambda}^{(j)}$, although there are some local peaks that are not.

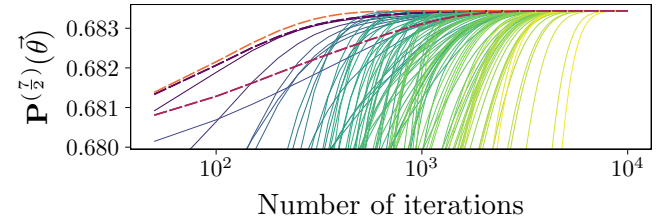


FIG. 15. Convergence to local maximum with the number of iterations. By choosing the initial parameters $(\vec{\theta}_{\Delta}^{(j)} + \vec{\theta}_K)/2$ for the gradient descent, shown with bolder lines, large violations can be found much faster than choosing random initial parameters.

We also studied the family of protocols when applied to spin angular momentum. There, we found that the quantum violation can be increased for a given spin system by adjusting the probing angles, and observed that the location of the local maxima in parameter space followed the pattern of the triangle numbers. The latter observation came from the fact that the optimal probing angles are close to a mixture of probing angles that reflect the symmetry of the protocol and that of the given spin, which also gives us an approximation of the optimal probing angles. This will be useful for choosing the probing angles in experimental implementations of the precession protocol, as recently demonstrated [8].

Afterwards, we related our findings to some previous results on the connection between the precession protocol and witnesses of entanglement. We show that similar to the original protocol, every member of the generalised family is an entanglement witness when applied to the collective coordinate of coupled harmonic oscillators or

spin ensembles. For the coupled harmonic oscillator, we further show that the separable bounds for every generalised protocol is the same as that of the original protocol. For both systems, we show by explicit examples that there are entangled states that can only be detected with the generalised protocol and not the original one. Therefore, this work also introduces new non-Gaussian and genuine multipartite entanglement witnesses.

Finally, we briefly touched upon precession protocols with more than three angles. We show that some results—like the classical bound and upper bound of the maximum quantum score—can be generalised to protocols with more angles, but also comment upon some results—like the invariance of the maximum quantum score for the harmonic oscillator—that cannot. We further demonstrate how observations from the three angle case can inform strategies for finding larger violations for the precession protocol with more angles.

There are some evident future directions: the first is to extend our work to larger K . The complexity grows very

quickly, as the parameter space of $K = 5$ is already four dimensional, with the different regions taking more complicated forms. The second is to extend this work to general theories, as has been done for the original protocol [7]. We note that our proof that the maximum harmonic oscillator score is the same for all three-angle generalisations depend only on symplectic transformations on the measured observables. Thus, our result also holds for the recently-introduced general theories based on continuous variable quasiprobability distributions, since these distributions also permit symplectic transformations [26, 27].

ACKNOWLEDGMENTS

This work is supported by the National Research Foundation, Singapore, and A*STAR under its CQT Bridging Grant. The computation involved in this work is supported by NUS IT's Research Computing group under the grant NUSREC-HPC-00001.

-
- [1] P. Ehrenfest, Bemerkung über die angenäherte Gültigkeit der klassischen mechanik innerhalb der Quantenmechanik, *Zeitschrift für Physik* **45**, 455 (1927).
- [2] B. Tsirelson, How often is the coordinate of a harmonic oscillator positive? (2006), [arXiv:quant-ph/0611147 \[quant-ph\]](#).
- [3] C. Emary, N. Lambert, and F. Nori, Leggett–Garg inequalities, *Reports on Progress in Physics* **77**, 016001 (2013).
- [4] C. Budroni, A. Cabello, O. Gühne, M. Kleinmann, and J.-A. Larsson, Kochen–Specker contextuality, *Rev. Mod. Phys.* **94**, 045007 (2022).
- [5] R. F. Werner, Wigner quantisation of arrival time and oscillator phase, *Journal of Physics A: Mathematical and General* **21**, 4565 (1988).
- [6] L. H. Zaw, C. C. Aw, Z. Lasmar, and V. Scarani, Detecting quantumness in uniform precessions, *Phys. Rev. A* **106**, 032222 (2022).
- [7] L. H. Zaw, M. Weilenmann, and V. Scarani, A theory-independent bound saturated by quantum mechanics (2024), [arXiv:2401.16147 \[quant-ph\]](#).
- [8] A. Vaartjes, M. Nurizzo, L. H. Zaw, B. Wilhelm, X. Yu, D. Holmes, D. Schwienbacher, A. Kringhøj, M. R. van Blankenstein, A. M. Jakob, F. E. Hudson, K. M. Itoh, R. J. Murray, R. Blume-Kohout, N. Anand, A. S. Dzurak, D. N. Jamieson, V. Scarani, and A. Morello, Certifying the quantumness of a single nuclear spin qudit through its uniform precession (2024), [arXiv:2410.07641 \[quant-ph\]](#).
- [9] P. Jayachandran, L. H. Zaw, and V. Scarani, Dynamics-based entanglement witnesses for non-gaussian states of harmonic oscillators, *Phys. Rev. Lett.* **130**, 160201 (2023).
- [10] K.-N. Huynh-Vu, L. H. Zaw, and V. Scarani, Certification of genuine multipartite entanglement in spin ensembles with measurements of total angular momentum, *Phys. Rev. A* **109**, 042402 (2024).
- [11] L. H. Zaw and V. Scarani, Dynamics-based quantumness certification of continuous variables using time-independent hamiltonians with one degree of freedom, *Phys. Rev. A* **108**, 022211 (2023).
- [12] M. Plávala, T. Heinosaari, S. Nimmrichter, and O. Gühne, Tsirelson inequalities: Detecting cheating and quantumness in a single framework, *Phys. Rev. A* **109**, 062216 (2024).
- [13] A. J. Bracken and G. F. Melloy, Probability backflow and a new dimensionless quantum number, *Journal of Physics A: Mathematical and General* **27**, 2197 (1994).
- [14] D. Trillo, T. P. Le, and M. Navascués, Quantum advantages for transportation tasks - projectiles, rockets and quantum backflow, *npj Quantum Information* **9**, 69 (2023).
- [15] C. K. Zachos, D. B. Fairlie, and T. L. Curtright, *Quantum Mechanics in Phase Space* (WORLD SCIENTIFIC, 2005).
- [16] A. Kenfack and K. Życzkowski, Negativity of the Wigner function as an indicator of non-classicality, *J. Opt. B* **6**, 396 (2004).
- [17] R. Takagi and Q. Zhuang, Convex resource theory of non-Gaussianity, *Phys. Rev. A* **97**, 062337 (2018).
- [18] F. Albarelli, M. G. Genoni, M. G. A. Paris, and A. Ferraro, Resource theory of quantum non-Gaussianity and Wigner negativity, *Phys. Rev. A* **98**, 052350 (2018).
- [19] J. G. Wood and A. J. Bracken, Bounds on integrals of the Wigner function: The hyperbolic case, *Journal of Mathematical Physics* **46**, 042103 (2005).
- [20] J. C. Várilly and J. Gracia-Bondía, Theoyal representation for spin, *Annals of Physics* **190**, 107 (1989).
- [21] S. Liu, J. Guo, Q. He, and M. Fadel, Quantum entanglement in phase space (2024), [arXiv:2409.17891 \[quant-ph\]](#).
- [22] L. H. Zaw, Certifiable lower bounds of wigner negativity volume and non-gaussian entanglement with conditional displacement gates, *Phys. Rev. Lett.* **133**, 050201 (2024).
- [23] T. Hillmann and F. Quijandría, Quantum error cor-

rection with dissipatively stabilized squeezed-cat qubits, *Phys. Rev. A* **107**, 032423 (2023).

- [24] Q. Xu, G. Zheng, Y.-X. Wang, P. Zoller, A. A. Clerk, and L. Jiang, Autonomous quantum error correction and fault-tolerant quantum computation with squeezed cat qubits, *npj Quantum Inf.* **9**, 78 (2023).
- [25] J. Chen, J. Tiong, L. H. Zaw, and V. Scarani, An even-parity precession protocol for detecting nonclassicality and entanglement (2024), [arXiv:2405.17966 \[quant-ph\]](https://arxiv.org/abs/2405.17966).
- [26] M. Plávala and M. Kleinmann, Operational Theories in Phase Space: Toy Model for the Harmonic Oscillator, *Phys. Rev. Lett.* **128**, 040405 (2022).
- [27] L. Jiang, D. R. Terno, and O. Dahlsten, Framework for generalized hamiltonian systems through reasonable postulates, *Phys. Rev. A* **109**, 032218 (2024).
- [28] H. Chen, On the summation of subseries in closed form, *International Journal of Mathematical Education in Science and Technology* **41**, 538 (2010).

Appendix A1: Proof of Classical Bound

In this appendix, we present the proof of the classical bound for the general precession protocol that involves probing at K arbitrary angles, with K odd. Collect the measured angles in the vector $\vec{\theta} := (\theta_k)_{k=1}^{K-1}$ with $0 =: \theta_0 \leq \theta_1 \leq \dots \leq \theta_{K-1} \leq 2\pi$. That is, we place all the angles in a circle and label them in increasing order in a clockwise direction.

Theorem A1. *The classical bound is $\mathbf{P}^c(\vec{\theta}) = 1 - \delta/K$ for $\delta \in \{0, 1, \dots, (K-1)/2\}$ if and only if*

$$\forall k : \theta_{(k \oplus_K \delta)} \ominus_{2\pi} \theta_k \leq \pi. \quad (\text{A1})$$

Proof. For any initial classical state $(A_x(0), A_y(0))$, the K points will take angles $\phi_0 + \theta_k$ with $\phi_0 := \text{atan}(A_y(0), A_x(0))$. Let $\phi_0 + \theta_{k_0}$ be the point in the $A_x > 0 \wedge A_y < 0$ plane closest to the A_y axis.

“*if*”: If $(\phi_0 + \theta_{k_0 \oplus_K \delta}) \ominus_{2\pi} (\phi_0 + \theta_{k_0}) \leq \pi$, this means that there must be at least $1 + \delta$ points on the left of a straight line from $\phi_0 + \theta_{k_0}$ to the origin, which means that there must be at least δ points on the negative A_x plane, which therefore implies that there must be at most $K - \delta$ points on the positive A_x plane. Since this is true for every ϕ_0 , Eq. (A1) implies

$$P^c(\vec{\theta}) \leq \mathbf{P}^c(\vec{\theta}) = \frac{K - \delta}{K} = 1 - \frac{\delta}{K}. \quad (\text{A2})$$

“*only if*”: Assume Eq. (A1) is false. Then, there is some k_0 such that $\theta_{k_0 \oplus_K \delta} \ominus_{2\pi} \theta_{k_0} > \pi$. We can choose a ϕ_0 such that both $\phi_0 + \theta_{k_0 \oplus_K \delta}$ and $\phi_0 + \theta_{k_0}$ are in the positive A_x plane, as the angle from the former to the latter in the anticlockwise direction is less than π . Since there are $K - \delta - 1$ points between the former and latter points excluding those two points, which would all be in the positive A_x plane, the score would be

$$P^c(\vec{\theta}) = \frac{(K - \delta - 1) + 2}{K} = \left(1 - \frac{\delta}{K}\right) + \frac{1}{K}, \quad (\text{A3})$$

so $\mathbf{P}^c(\vec{\theta}) \geq P^c(\vec{\theta}) > 1 - \delta/K$. Taking the converse, $\mathbf{P}^c(\vec{\theta}) \leq 1 - \delta/K$ implies Eq. (A1). \square

Appendix A2: Transformation Between Three-angle Generalisations of Tsirelson’s Precession Protocol with the Quantum Harmonic Oscillator

Theorem A2. $\mathbf{P}^\infty(\vec{\theta}) = 2/3$ on the boundary of the $\mathbf{P}^c(\vec{\theta}) = 2/3$ region.

Proof. On the boundary, exactly one or two of Eq. (5) is satisfied: so, at least one inequality will be saturated and at least one other will be strict. By Eq. (6), all such boundaries are equivalent. Consider the one defined by $\theta_1 = \pi$ and $\theta_2 - \theta_1 < \pi$. Then,

$$\begin{aligned} Q^\infty(\vec{\theta}) &= \frac{1}{3} \left\{ \underbrace{\Theta(X) + \Theta(-X)}_1 + \Theta[X(\theta_2)] \right\} \\ &= \frac{1}{3} \mathbb{1} + \frac{1}{3} \Theta[X(\theta_2)]. \end{aligned} \quad (\text{A1})$$

Since $\langle \Theta[X(\theta_2)] \rangle \leq 1$, this gives $\mathbf{P}^\infty \leq 2/3$, which is saturated by any state with only positive support on $X(\theta_2)$. \square

Theorem A3. $\mathbf{P}^\infty(\vec{\theta}) = \mathbf{P}_3^\infty$ in the interior region Δ where $\mathbf{P}^c(\vec{\theta}) = 2/3$.

Proof. The constructive proof involves showing that $Q^\infty(\vec{\theta}) = U(\vec{\theta})Q_3^\infty U^\dagger(\vec{\theta})$ for a symplectic unitary $U(\vec{\theta})$, which leaves the maximum eigenvalue unchanged. Explicitly, $U(\vec{\theta}) = R_{\phi_0} S_{\lambda_1} R_{\phi_2} S_{\lambda_3}$ is a sequence of squeeze operators $S_\lambda := \exp[-i\lambda(XP + PX)/2]$ and rotation operators $R_\phi := \exp[-i\phi(X^2 + P^2)/2]$, which act on a general quadrature $X(\theta) = X \cos \theta + P \sin \theta$ as

$$\begin{aligned} S_\lambda^\dagger X(\theta) S_\lambda &= X e^\lambda \cos \theta + P e^{-\lambda} \sin \theta, \\ R_\phi^\dagger X(\theta) R_\phi &= X \cos(\theta - \phi) + P \sin(\theta - \phi). \end{aligned} \quad (\text{A2})$$

We shall break it down into several steps. First, defining

$$\phi_0 := \begin{cases} 0 & \text{if } (\pi < \theta_2 \leq 2\theta_1) \wedge (\frac{\pi}{2} < \theta_1 \leq \frac{2\pi}{3}) \\ & \text{or } (\pi < \theta_2 \leq \frac{\theta_1}{2} + \pi) \wedge (\frac{2\pi}{3} \leq \theta_1 < \pi) \\ \theta_1 & \text{if } (2\pi - \theta_1 \leq \theta_2 < \pi + \theta_1) \wedge (\frac{\pi}{2} < \theta_1 \leq \frac{2\pi}{3}) \\ & \text{or } (\frac{\theta_1}{2} + \pi \leq \theta_2 < \pi + \theta_1) \wedge (\frac{2\pi}{3} \leq \theta_1 < \pi) \\ \theta_2 & \text{if } (2\theta_1 \leq \theta_2 \leq 2\pi - \theta_1) \wedge (\frac{\pi}{2} < \theta_1 \leq \frac{2\pi}{3}) \\ & \text{or } (\pi < \theta_2 < \pi + \theta_1) \wedge (0 < \theta_1 \leq \frac{\pi}{2}) \end{cases} \quad (\text{A3})$$

we have $R_{\phi_0}^\dagger Q^\infty(\vec{\theta}) R_{\phi_0} = Q^\infty(\theta'_1, \theta'_2)$, where

$$\theta'_1 = \begin{cases} \theta_1 & \text{if } \phi_0 = 0, \\ \theta_2 - \theta_1 & \text{if } \phi_0 = \theta_1, \\ 2\pi - \theta_2 & \text{if } \phi_0 = \theta_2; \end{cases} \quad (\text{A4})$$

and

$$\theta'_2 = \begin{cases} \theta_1 & \text{if } \phi_0 = 0, \\ 2\pi - \theta_1 & \text{if } \phi_0 = \theta_1, \\ 2\pi - (\theta_2 - \theta_1) & \text{if } \phi_0 = \theta_2. \end{cases} \quad (\text{A5})$$

This transformation essentially uses the symmetry in Eq. (6) to bring every point in the interior of the $\mathbf{P}_3^\infty = 2/3$ region onto the bottom right trine of the purple tri-

angle in Fig. 1(b), for which $(\pi/2 < \theta'_1 < \pi) \wedge (\pi < \theta'_2 < 3\pi/2)$. Then, defining

$$\lambda_1 := \frac{1}{4} \log \left(\frac{\tan^2 \theta'_1 \tan \theta'_2}{\tan \theta'_2 - 2 \tan \theta'_1} \right), \quad (\text{A6})$$

which is well-defined because $\tan \theta_2 > 0$ and $\tan \theta_1 < 0$ in this region, so the argument in the logarithm is strictly positive. This gives

$$\begin{aligned} S_{\lambda_1}^\dagger Q^\infty(\theta'_1, \theta'_2) S_{\lambda_1} &= \frac{1}{3} \left[\Theta(Xe^{\lambda_1}) + \Theta(Xe^{\lambda_1} \cos \theta'_1 + Pe^{-\lambda_1} \sin \theta'_1) + \Theta(Xe^{\lambda_1} \cos \theta'_2 + Pe^{-\lambda_1} \sin \theta'_2) \right] \\ &=: \frac{1}{3} \left[\Theta(X) + \Theta(X \cos \theta''_1 + P \sin \theta''_1) + \Theta(X \cos \theta''_2 + P \sin \theta''_2) \right] \\ &= Q^\infty(\theta''_1, \theta''_2), \end{aligned} \quad (\text{A7})$$

where we used $\Theta(x) = \Theta(cx)$ for any $c > 0$ and defined $\theta''_k := \text{atan}(e^{-\lambda_1} \sin \theta'_k, e^{\lambda_1} \cos \theta'_k) \bmod 2\pi$ for $k = 1, 2$. Substituting Eq. (A6) into the definition of θ''_k ,

$$\begin{aligned} \theta''_1 &= \text{atan}(e^{-\lambda_1} \sin \theta'_1, e^{\lambda_1} \cos \theta'_1) \bmod 2\pi \\ &= \pi - \text{atan} \sqrt{1 + \frac{2|\tan \theta'_1|}{\tan \theta'_2}} \\ &= \frac{\pi}{2} + \text{atan} \frac{1}{\sqrt{1 + 2|\tan \theta'_1|/\tan \theta'_2}} \\ &=: \phi_2, \end{aligned} \quad (\text{A8a})$$

$$\begin{aligned} \theta''_2 &= \text{atan}(e^{-\lambda_1} \sin \theta'_2, e^{\lambda_1} \cos \theta'_2) \bmod 2\pi \\ &= \pi + \text{atan} \frac{\sqrt{1 + 2|\tan \theta'_1|/\tan \theta'_2}}{|\tan \theta'_1|/\tan \theta'_2} \\ &= 2 \left(\frac{\pi}{2} + \text{atan} \frac{1}{\sqrt{1 + 2|\tan \theta'_1|/\tan \theta'_2}} \right) \\ &= 2\phi_2, \end{aligned} \quad (\text{A8b})$$

where we have used $\text{atan}(x) + \text{atan}(1/x) = \pi/2$ and $2 \text{atan}(1/\sqrt{2x+1}) = \text{atan}(\sqrt{2x+1}/x)$ for $x > 0$; the latter identity can be proven by taking the tangent on both sides and using the double angle formula. This therefore implies that $S_{\lambda_1}^\dagger Q^\infty(\theta'_1, \theta'_2) S_{\lambda_1} = Q^\infty(\phi_2, 2\phi_2)$, where $\pi/2 < \phi_2 < 3\pi/4$ as $|\tan \theta'_1|/\tan \theta'_2$ is finite and strictly positive in this region.

Finally, by defining $4\lambda_3 := 2 \log |\tan \phi_2| - \log 3$,

$$\begin{aligned} S_{\lambda_3}^\dagger R_{\phi_2}^\dagger Q^\infty(\phi_2, 2\phi_2) R_{\phi_2} S_{\lambda_3} &= \frac{1}{3} \left[\Theta(Xe^{\lambda_3} \cos \phi_2 - Pe^{-\lambda_3} \sin \phi_2) + \Theta(X) \right. \\ &\quad \left. + \Theta(Xe^{\lambda_3} \cos \phi_2 + Pe^{-\lambda_3} \sin \phi_2) \right] \\ &= Q^\infty(\tilde{\theta}_+, \tilde{\theta}_-), \end{aligned} \quad (\text{A9})$$

where similar to before we have defined $\tilde{\theta}_\pm := \text{atan}(\pm e^{-\lambda_3} \sin \phi_2, e^{\lambda_3} \cos \phi_2) \bmod 2\pi$. Since $\pi/2 < \phi_2 < 3\pi/4 \implies \tan \phi_2 = -|\tan \phi_2|$,

$$\begin{aligned} \tilde{\theta}_\pm &= \pi \mp \text{atan} |e^{-2\lambda_3} \tan \theta| \\ &= \pi \mp \text{atan} \sqrt{3} \\ &= \begin{cases} 2\pi/3 & \text{for } \tilde{\theta}_+, \\ 4\pi/3 & \text{for } \tilde{\theta}_-. \end{cases} \end{aligned} \quad (\text{A10})$$

Hence, $S_{\lambda_3}^\dagger R_{\phi_2}^\dagger Q^\infty(\phi_2, 2\phi_2) R_{\phi_2} S_{\lambda_3} = Q^\infty(2\pi/3, 4\pi/3) = Q_3^\infty$. Putting everything together,

$$Q^\infty(\vec{\theta}) = \underbrace{R_{\phi_0} S_{\lambda_1} R_{\phi_2} S_{\lambda_3}}_{=: U(\vec{\theta})} Q_3^\infty S_{\lambda_3}^\dagger R_{\phi_2}^\dagger S_{\lambda_1}^\dagger R_{\phi_0}^\dagger, \quad (\text{A11})$$

with $\phi_0, \lambda_1, \phi_2$, and λ_3 as defined above. Since this shows that Q_3^∞ and $Q^\infty(\vec{\theta})$ are related by the unitary transformation $U(\vec{\theta})$, which leaves the eigenvalues unchanged, this implies that $\mathbf{P}^\infty(\vec{\theta}) = \mathbf{P}_3^\infty$, which completes the proof. Note that this also means that if the state $|P_3\rangle$ obtains the score P_3 for the original protocol, then the state $U(\vec{\theta})|P_3\rangle$ obtains the same score for the protocol with probing angles $\vec{\theta}$. \square

Appendix A3: Lower Bound Expressions

The matrix element of $\Theta(X) - \mathbb{1}/2$ is known to be [6]

$$\langle n | \left(\Theta(X) - \frac{1}{2} \mathbb{1} \right) | n' \rangle = \begin{cases} 0 & \text{if } n \ominus_2 n' = 0, \\ \frac{(-1)^{\frac{n-n'-1}{2}} 2^{-\frac{n+n'}{2}}}{n-n'} \sqrt{\frac{n(n \bmod 2) n'(n' \bmod 2)}{\pi} \binom{2 \lfloor \frac{n}{2} \rfloor}{\frac{n}{2}} \binom{2 \lfloor \frac{n'}{2} \rfloor}{\lfloor \frac{n'}{2} \rfloor}} & \text{otherwise,} \end{cases} \quad (\text{A1})$$

while $Q_3^\infty - \mathbb{1}/2$ is given by the direct sum

$$Q_3^\infty - \frac{1}{2} \mathbb{1} = \bigoplus_{k=0}^2 \left[\Pi_{k|3}^- \left(\Theta(X) - \frac{1}{2} \mathbb{1} \right) \Pi_{k|3}^+ + \Pi_{k|3}^+ \left(\Theta(X) - \frac{1}{2} \mathbb{1} \right) \Pi_{k|3}^- \right], \quad (\text{A2})$$

where $\Pi_{k|3}^+ := \sum_{n=0}^{\infty} |6n+k\rangle\langle 6n+k|$ and $\Pi_{k|3}^- := \sum_{n=0}^{\infty} |6n+3+k\rangle\langle 6n+3+k|$. Since $A_3 = (Q_3^\infty - \frac{1}{2} \mathbb{1})^2 - (\mathbf{P}_3^c - \frac{1}{2})^2 \mathbb{1}$,

$$\langle 6n+k | A_3 | 6n'+k \rangle = \sum_{m=0}^{\infty} \langle 6n+k | \left(\Theta(X) - \frac{1}{2} \mathbb{1} \right) | 6m+k+3 \rangle \langle 6m+k+3 | \left(\Theta(X) - \frac{1}{2} \mathbb{1} \right) | 6n'+k \rangle - \delta_{n,n'} \left(\mathbf{P}_3^c - \frac{1}{2} \right)^2 \quad (\text{A3})$$

with $k \in \{0, 1, 2\}$. Let us first consider k even. Then, we can write Eq. (A3) as the sum $\sum_{m=0}^{\infty} c_{3m+(1+k/2)}^{n,n'} = \sum_{m \bmod 3=1+k/2}^{\infty} c_m^{n,n'}$, where

$$c_m^{n,n'} := \langle 6n+k | \left(\Theta(X) - \frac{1}{2} \mathbb{1} \right) | 2m+1 \rangle \langle 2m+1 | \left(\Theta(X) - \frac{1}{2} \mathbb{1} \right) | 6n'+k \rangle. \quad (\text{A4})$$

In other words, Eq. (A3) is a subseries of the series $\{c_m^{n,n'}\}_{m=0}^{\infty}$, so the matrix element can be rewritten as [28]

$$\langle 6n+k | A_3 | 6n'+k \rangle = \frac{1}{3} \sum_{j=0}^2 e^{-i \frac{2\pi j}{3} (1+\frac{k}{2})} \left[\sum_{m=0}^{\infty} c_m^{3n+\frac{k}{2}, 3n'+\frac{k}{2}} \left(e^{i \frac{2\pi j}{3}} \right)^m \right] - \delta_{n,n'} \left(\mathbf{P}_3^c - \frac{1}{2} \right)^2. \quad (\text{A5})$$

The full series in the square bracket can be interpreted as the Maclaurin series of a function with the argument $e^{i(2\pi j/3)}$. Isolating the parts of the function where the series needs to be resolved, we have

$$\sum_{m=0}^{\infty} c_m^{n,n'} z^m = \frac{(-1)^{n+n'} 2^{-(n+n')}}{8\pi} \sqrt{\binom{2n}{n} \binom{2n'}{n'}} \underbrace{\sum_{m=0}^{\infty} \binom{2m}{m} \frac{2(m+\frac{1}{2}) 2^{-2m}}{((m-n)+\frac{1}{2})((m-n')+\frac{1}{2})}}_{:=l(z;n,n')} z^m. \quad (\text{A6})$$

Finally, by using the series definitions of the generalised hypergeometric function ${}_3F_2(a_1, a_2, a_3; b_1, b_2; z) = \sum_{n=0}^{\infty} \frac{(a_1+n-1)!(a_2+n-1)!(a_3+n-1)!(b_1-1)!(b_2-1)!}{(b_1+n-1)!(b_2+n-1)!(a_1-1)!(a_2-1)!(a_3-1)!} \frac{z^n}{n!}$ and the incomplete beta function $B(z; a, b) = \int_0^z t^{a-1} (1-t)^{b-1} dt = \sum_{n=0}^{\infty} \frac{(n-b)! z^{n+a}}{(-b)! n! (n+a)}$, we obtain

$$l(z; n, n') = \begin{cases} \frac{{}_3F_2(\frac{1}{2}, \frac{1}{2}-n, \frac{1}{2}-n; \frac{3}{2}-n, \frac{3}{2}-n; z)}{(\frac{1}{2}-n)^2} + \frac{z {}_3F_2(\frac{3}{2}, \frac{3}{2}-n, \frac{3}{2}-n; \frac{5}{2}-n, \frac{5}{2}-n; z)}{(\frac{3}{2}-n)^2} & \text{if } n = n', \\ \frac{z^{n'-1/2}}{n'} B(z; \frac{1}{2} - n', \frac{1}{2}) & \text{if } 0 = n \neq n', \\ \frac{z^{n-1/2}}{n} B(z; \frac{1}{2} - n, \frac{1}{2}) & \text{if } n \neq n' = 0, \\ (2n) \frac{z^{n-1/2}}{n-n'} B(z; \frac{1}{2} - n, -\frac{1}{2}) + (2n') \frac{z^{n'-1/2}}{n'-n} B(z; \frac{1}{2} - n', -\frac{1}{2}) & \text{otherwise.} \end{cases} \quad (\text{A7})$$

With this, for k even, the matrix elements of A_3 is

$$\langle 6n+k | A_3 | 6n'+k \rangle = \frac{(-1)^{(n+n')} 2^{-(3(n+n')+k)}}{24\pi} \sqrt{\binom{6n+k}{3n+\frac{k}{2}} \binom{6n'+k}{3n'+\frac{k}{2}}} \sum_{j=0}^2 e^{-i \frac{2\pi j}{3} (1+\frac{k}{2})} l(e^{i \frac{2\pi j}{3}}; 3n+\frac{k}{2}, 3n'+\frac{k}{2}) - \delta_{n,n'} \left(\mathbf{P}_3^c - \frac{1}{2} \right)^2, \quad (\text{A8})$$

and similar steps for k odd give

$$\langle 6n+3+k | A_3 | 6n'+3+k \rangle = \frac{(-1)^{(n+n')} 2^{-(3(n+n'+1)+k)}}{24\pi} \sqrt{\binom{6n+3+k}{3n+\frac{3+k}{2}} \binom{6n'+3+k}{3n'+\frac{3+k}{2}}} \times \sum_{j=0}^2 e^{-i \frac{2\pi j}{3} (\frac{k-1}{2})} l(e^{i \frac{2\pi j}{3}}; 3n+\frac{3+k}{2}, 3n'+\frac{3+k}{2}) - \delta_{n,n'} \left(\mathbf{P}_3^c - \frac{1}{2} \right)^2. \quad (\text{A9})$$

Appendix A4: Upper Bound Expressions

In Sec. III B of the main text, the inequality $2(\mathbf{P}_3^\infty - \frac{2}{3})^2(\mathbf{P}_3^\infty - \frac{1}{3})^2 \leq \text{tr}(A_3^2)$ was found by using the double degeneracies of the nonzero eigenvalues of A_3 and the relationship between the eigenvalues of Q_3^∞ and A_3 . In this appendix, we detail the steps required to obtain the exact value of the latter expression.

To do so, we require the formalism of Wigner functions. For a continuous variable system with a single degree of freedom, recall that the Wigner function of a state ρ is defined as [15]

$$W_\rho(x, p) := \frac{1}{2\pi i} \text{tr} \left(\rho e^{i\frac{\pi}{2}[(X-x)^2 + (P-p)^2]} \right), \quad (\text{A1})$$

while the Wigner function of an observable A is the function $W_A(x, p)$ that satisfies $\text{tr}(A\rho) = \int dx \int dp W_A(x, p) W_\rho(x, p)$ for every state ρ , which may be defined in the sense of a distribution. The Wigner function of $\Theta[X(\theta)] \circ \Theta[X(\theta')] := \frac{1}{2}(\Theta[X(\theta)]\Theta[X(\theta')] + \Theta[X(\theta')]\Theta[X(\theta)])$, where $X(\theta) = X \cos \theta + P \sin \theta$, was

derived by Tsirelson to be [2]

$$W_{\Theta[X(\theta)] \circ \Theta[X(\theta')]}(x, p) = \frac{1}{2} (\Theta[x(\theta)] + \Theta[x(\theta')]) + \frac{1}{2\pi} \text{si} \left[\frac{2x(\theta)x(\theta')}{|\sin(\theta - \theta')|} \right], \quad (\text{A2})$$

where $\text{si}(x) = -\int_x^\infty dt \frac{\sin t}{t}$ and $x(\theta) = x \cos \theta + p \sin \theta$. A few special values of $\text{si}(x)$ are $\text{si}(-\infty) = \pi$, $\text{si}(0) = \pi/2$, and $\text{si}(\infty) = 0$, which come from standard integrals of $\sin(x)/x$. The last special value also implies that $W_{(\Theta[X(\theta)])^2}(x, p) = \Theta[x(\theta)]$, which is the expected result coming from $(\Theta[X(\theta)])^2 = \Theta[X(\theta)]$

Using Eq. (A2), the Wigner function of $A_3 = (Q_3^\infty - \frac{2}{3}\mathbb{1})(Q_3^\infty - \frac{1}{3}\mathbb{1})$ can be found to be

$$W_{A_3}(x, p) = \frac{2}{9} + \frac{1}{18} \sum_{k=0}^2 \frac{2}{\pi} \text{si} \left[\frac{4}{\sqrt{3}} x \left(\frac{2\pi k}{3} \right) x \left(\frac{2\pi(k+1)}{3} \right) \right]. \quad (\text{A3})$$

In terms of their Wigner functions, the trace of two observables is given by

$$\text{tr}(AB) = \frac{1}{2\pi} \int dx \int dp W_A(x, p) W_B(x, p), \quad (\text{A4})$$

with which we calculate $\text{tr}(A_3^2)$ to be

$$\begin{aligned} \text{tr}(A_3^2) &= \frac{1}{2\pi} \int_{-\infty}^{\infty} dx \int_{-\infty}^{\infty} dp [W_{A_3}(x, p)]^2 \\ &= \frac{1}{2\pi} \int_{-\infty}^{\infty} dx \int_{-\infty}^{\infty} dp \left\{ \frac{2}{9} + \frac{1}{18} \sum_{k=0}^2 \frac{2}{\pi} \text{si} \left[\frac{4}{\sqrt{3}} x \left(\frac{2\pi k}{3} \right) x \left(\frac{2\pi(k+1)}{3} \right) \right] \right\}^2 \\ &= \frac{1}{162\pi^3} \int_{-\infty}^{\infty} dx \int_{-\infty}^{\infty} dp \left\{ \sum_{k=0}^2 (-1)^{\delta_{k,1}} \text{si} \left[-(-1)^{\delta_{k,1}} \frac{4}{\sqrt{3}} x \left(\frac{2\pi k}{3} \right) x \left(\frac{2\pi(k+1)}{3} \right) \right] \right\}^2 \\ &= \frac{1}{324\pi^3} \int_{-\pi}^{\pi} d\phi \int_0^{\infty} d[r^2] \left\{ \text{si} \left[\frac{4r^2}{\sqrt{3}} \cos\left(\phi + \frac{\pi}{3}\right) \cos\left(\phi - \frac{\pi}{3}\right) \right] - \sum_{\sigma \in \{+, -\}} \text{si} \left[\frac{4r^2}{\sqrt{3}} \cos(\phi) \cos\left(\phi + \sigma \frac{\pi}{3}\right) \right] \right\}^2 \\ &= \frac{1}{27\pi^3} \int_0^{\frac{\pi}{6}} d\phi \int_0^{\infty} d[r^2] \left\{ \text{si} \left[\frac{4r^2}{\sqrt{3}} \cos\left(\phi + \frac{\pi}{3}\right) \cos\left(\phi - \frac{\pi}{3}\right) \right] - \sum_{\sigma \in \{+, -\}} \text{si} \left[\frac{4r^2}{\sqrt{3}} \cos(\phi) \cos\left(\phi + \sigma \frac{\pi}{3}\right) \right] \right\}^2, \end{aligned} \quad (\text{A5})$$

where we have used $\text{si}(-x) = -\text{si}(x) - \text{si}(-\infty) = -\text{si}(x) - \pi$ in the second line. In the penultimate line, a change of variables to radial coordinates $x = r \cos \phi$ and $p = r \sin \phi$ was performed, and we also used the identity $-\cos(x) = \cos(x - \pi)$; in the last line, we used the fact that the integrand is symmetric under the transformations $\phi \rightarrow \phi + \pi/3$ and $\phi \rightarrow -\phi$, which implies that the integral over $-\pi < \phi < \pi$ is simply 12 times of the integral over $0 < \phi < \pi/6$.

The integration over the radial variable involve integrals of the form $\int_0^L dx \text{si}(ax) \text{si}(bx)$ for some $0 < a \leq b < \infty$. We can evaluate the integral $\int_0^L dx \text{si}(ax) \text{si}(bx)$, where we will later take $L \rightarrow \infty$, to be

$$\int_0^L dx \text{si}(ax) \text{si}(bx) = \frac{\pi}{2b} + \text{si}(aL) \text{si}(bL)L - \frac{b-a}{2ab} \text{si}[(b-a)L] - \frac{b+a}{2ab} \text{si}[(b+a)L] + \frac{\cos(aL)}{a} \text{si}(bL) + \frac{\cos(bL)}{b} \text{si}(aL), \quad (\text{A6})$$

which can be verified by taking the derivative on both sides with respect to L using $\frac{d}{dL} \text{si}(cL) = \sin(cL)/L$ and

also confirming that both sides of the equation are zero when $L = 0$ using $\text{si}(0) = \pi/2$.

Now, to take the limit $L \rightarrow \infty$, we first take care of the troublesome term $\text{si}(aL)\text{si}(bL)L$ using integration by parts to find that

$$\begin{aligned}\sqrt{x}\text{si}(x) &= \sqrt{x} \int_x^\infty dt \frac{1}{t} \frac{d\cos(t)}{dt} \\ &= \sqrt{x} \left[\frac{\cos(t)}{t} \right]_x^\infty + \int_x^\infty dt \frac{\sqrt{x}\cos(t)}{t^2} \quad (\text{A7}) \\ &= -\frac{\cos(x)}{\sqrt{x}} + \int_x^\infty dt \frac{\sqrt{x}\cos(t)}{t^2},\end{aligned}$$

whose magnitude for $x > 0$ is therefore bounded as

$$\begin{aligned}|\sqrt{x}\text{si}(x)| &\leq \frac{|\cos(x)|}{\sqrt{x}} + \int_x^\infty dt \frac{\sqrt{x}|\cos(t)|}{t^2} \\ &\leq \frac{1}{\sqrt{x}} + \int_x^\infty dt \frac{1}{t^{3/2}} = \frac{3}{\sqrt{x}}.\end{aligned} \quad (\text{A8})$$

This implies that $\lim_{x \rightarrow \infty} |\sqrt{x}\text{si}(x)| \leq \lim_{x \rightarrow \infty} 3/\sqrt{x} = 0$, and thus $\lim_{L \rightarrow \infty} \text{si}(aL)\text{si}(bL)L = 0$. Every other term in Eq. (A6) that depend on L vanish due to $\lim_{L \rightarrow \infty} \text{si}(cL) = \text{si}(\infty) = 0$ when $c > 0$, which leaves only the first term $\pi/(2b)$. Therefore, $\int_0^\infty dx \text{si}(ax)\text{si}(bx) = \pi/(2b)$ for any $0 < a \leq b < \infty$.

To apply this to the integral over r^2 in Eq. (A5), we use the monotonicity of $\cos(x)$ within the range $0 \leq x \leq \pi$ to ascertain that $\cos(\phi + \frac{\pi}{3}) \leq \cos(\phi - \frac{\pi}{3}) \leq \cos(\phi)$ for $0 < \phi < \pi/6$, with which we can determine that

$$\begin{aligned}\frac{4}{\sqrt{3}} \cos(\phi + \frac{\pi}{3}) \cos(\phi - \frac{\pi}{3}) &\leq \frac{4}{\sqrt{3}} \cos(\phi) \cos(\phi + \frac{\pi}{3}) \\ &\leq \frac{4}{\sqrt{3}} \cos(\phi) \cos(\phi - \frac{\pi}{3})\end{aligned} \quad (\text{A9})$$

within the range of ϕ we will be integrating over. Finally, by making liberal use of the identities $\cos(a \pm b) = \cos(a)\cos(b) \mp \sin(a)\sin(b)$ and $\sin(a \pm b) = \sin(a)\cos(b) \pm \cos(a)\sin(b)$, and the special values $\cos(\pi/3) = 1/2$ and $\sin(\pi/3) = \sqrt{3}/2$, we end up with

$$\begin{aligned}\text{tr}(A_3^2) &= \frac{1}{27\pi^3} \int_0^{\pi/6} d\phi \left\{ \frac{\pi/2}{\frac{4}{\sqrt{3}} \cos(\phi + \frac{\pi}{3}) \cos(\phi - \frac{\pi}{3})} + \frac{\pi/2}{\frac{4}{\sqrt{3}} \cos(\phi) \cos(\phi + \frac{\pi}{3})} + \frac{\pi/2}{\frac{4}{\sqrt{3}} \cos(\phi) \cos(\phi - \frac{\pi}{3})} \right. \\ &\quad \left. - \frac{\pi}{\frac{4}{\sqrt{3}} \cos(\phi) \cos(\phi + \frac{\pi}{3})} - \frac{\pi}{\frac{4}{\sqrt{3}} \cos(\phi) \cos(\phi - \frac{\pi}{3})} + \frac{\pi}{\frac{4}{\sqrt{3}} \cos(\phi) \cos(\phi - \frac{\pi}{3})} \right\} \\ &= \frac{1}{72\sqrt{3}\pi^2} \int_0^{\pi/6} d\phi \frac{\cos(\phi) - \cos(\phi - \frac{\pi}{3}) + \cos(\phi + \frac{\pi}{3})}{\cos(\phi) \cos(\phi + \frac{\pi}{3}) \cos(\phi - \frac{\pi}{3})} \\ &= \frac{1}{72\sqrt{3}\pi^2} \int_0^{\pi/6} d\phi \frac{\cos(\phi) - 2\sin(\frac{\pi}{3})\sin(\phi)}{\cos(\phi) \cos(\phi + \frac{\pi}{3}) \cos(\phi - \frac{\pi}{3})} \\ &= \frac{1}{36\sqrt{3}\pi^2} \int_0^{\pi/6} d\phi \frac{\frac{1}{2}\cos(\phi) - \frac{\sqrt{3}}{2}\sin(\phi)}{\cos(\phi) \cos(\phi + \frac{\pi}{3}) \cos(\phi - \frac{\pi}{3})} \\ &= \frac{1}{36\sqrt{3}\pi^2} \int_0^{\pi/6} d\phi \frac{1}{\cos(\phi) \cos(\phi - \frac{\pi}{3})} \\ &= \frac{1}{54\pi^2} \int_0^{\pi/6} d\phi \left[\tan\left(\phi + \frac{\pi}{6}\right) - \tan\left(\phi - \frac{\pi}{6}\right) \right] \\ &= \frac{6 \log 2}{(18\pi)^2}.\end{aligned} \quad (\text{A10})$$

Appendix A5: Heuristic Optimisation of Local Maxima

We observed in Sec. IV A that the local maxima are close to, but not exactly at, the resonant angles $\vec{\theta}_\Delta^{(j)}(n_1, n_2) = (n_1\pi/j, n_2\pi/j)$. In this appendix, we shall numerically find the local maxima using $\vec{\theta}_\Delta^{(j)}$ as the initial point for the

gradient descent optimisation of $\mathbf{P}^{(j)}(\vec{\theta})$, The gradient of $\mathbf{P}^{(j)}(\vec{\theta})$ can be analytically found to be

$$\begin{aligned} \frac{\partial \mathbf{P}^{(j)}(\vec{\theta})}{\partial \theta_k} &= i \frac{1}{3} \langle \mathbf{P}^{(j)}(\vec{\theta}) | e^{-i\theta_k J_z} [\Theta(J_x), J_z] e^{i\theta_k J_z} | \mathbf{P}^{(j)}(\vec{\theta}) \rangle \\ &= \begin{cases} i \frac{\sqrt{j(j+1)}}{12} \langle \mathbf{P}^{(j)}(\vec{\theta}) | e^{-i\theta_k J_z} e^{-i\frac{\pi}{2} J_y} [|j, -1\rangle\langle j, 0| + |j, 0\rangle\langle j, 1| \\ \quad - |j, 1\rangle\langle j, 0| - |j, 0\rangle\langle j, -1|] e^{i\frac{\pi}{2} J_y} e^{i\theta_k J_z} | \mathbf{P}^{(j)}(\vec{\theta}) \rangle & \text{for } j \text{ integer,} \\ i \frac{j+1/2}{6} \langle \mathbf{P}^{(j)}(\vec{\theta}) | e^{-i\theta_k J_z} e^{-i\frac{\pi}{2} J_y} (|j, -\frac{1}{2}\rangle\langle j, \frac{1}{2}| - |j, \frac{1}{2}\rangle\langle j, -\frac{1}{2}|) e^{i\frac{\pi}{2} J_y} e^{i\theta_k J_z} | \mathbf{P}^{(j)}(\vec{\theta}) \rangle & \text{otherwise,} \end{cases} \end{aligned} \quad (\text{A1})$$

where $|\mathbf{P}^{(j)}(\vec{\theta})\rangle$ is the maximal eigenstate of $Q^{(j)}(\vec{\theta})$.

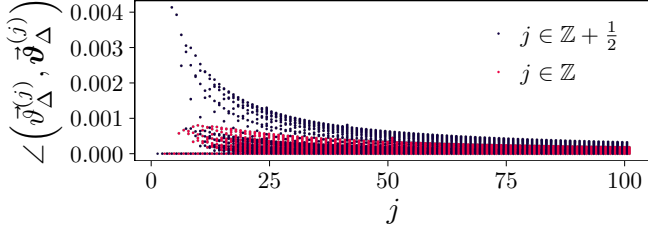


FIG. A1. The angle $\angle(\vec{\vartheta}_\Delta^{(j)}, \vec{\vartheta}_\Delta^{(j)})$ between the local peaks $\vec{\vartheta}_\Delta^{(j)}$ and the resonant probing angles $\vec{\vartheta}_\Delta^{(j)}$. We find that $\angle(\vec{\vartheta}_\Delta^{(j)}, \vec{\vartheta}_\Delta^{(j)}) \approx 0$, which shows that $\vec{\vartheta}_\Delta^{(j)}$ and $\vec{\vartheta}_\Delta^{(j)}$ are approximately scalar multiples of each other.

The local peaks $\vec{\vartheta}_\Delta^{(j)}$ as found are plotted alongside $\vec{\vartheta}_\Delta^{(j)}$ in Fig. A1, where they appear to be scalar multiples of each other. To investigate this further, we plotted the angle

$$\angle(\vec{\vartheta}_\Delta^{(j)}, \vec{\vartheta}_\Delta^{(j)}) = \text{acos} \left(\frac{\vec{\vartheta}_\Delta^{(j)} \cdot \vec{\vartheta}_\Delta^{(j)}}{|\vec{\vartheta}_\Delta^{(j)}| |\vec{\vartheta}_\Delta^{(j)}|} \right) \quad (\text{A2})$$

for a large range of j in Fig. A1. $\angle(\vec{\vartheta}_\Delta^{(j)}, \vec{\vartheta}_\Delta^{(j)}) \approx 0$ for all values that we calculated, which verifies that they are indeed roughly scalar multiples of each other.

With a phenomenological fit of the scaling factor, we also found $\vec{\vartheta}_\Delta^{(j)} \approx \lambda_j \vec{\vartheta}_\Delta^{(j)}$ to be an excellent approximation of the local maximum, where

$$\frac{1}{\lambda_j} = 1 + \begin{cases} \frac{0.533\,051}{j-0.213\,570} & \text{for } j \text{ integer,} \\ \frac{0.554\,086}{j-0.197\,425} & \text{otherwise.} \end{cases} \quad (\text{A3})$$

The discrepancy is at most $|\vec{\vartheta}_\Delta^{(j)} - \lambda_j \vec{\vartheta}_\Delta^{(j)}| \leq 0.004$ for $j \leq 100$, which decreases monotonically with j , as shown in Fig. A2.

Appendix A6: Separable Bounds of Coupled Harmonic Oscillators

Theorem A4. For all $\vec{\theta}$ in the region where $\mathbf{P}^c(\vec{\theta}) = 2/3$, $\mathbf{P}^{\infty\text{-sep}}(\varphi, \vec{\theta}) = \mathbf{P}_3^{\infty\text{-sep}}(\phi)$.

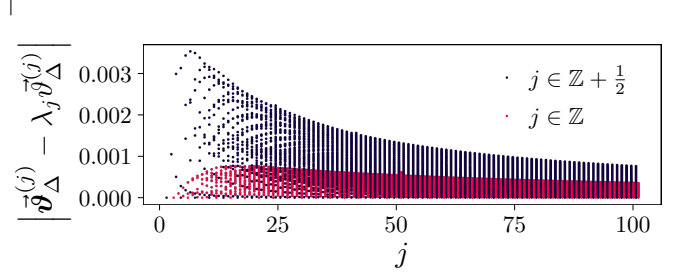


FIG. A2. The discrepancy $|\vec{\vartheta}_\Delta^{(j)} - \lambda_j \vec{\vartheta}_\Delta^{(j)}|$ between the local peaks $\vec{\vartheta}_\Delta^{(j)}$ and the rescaled resonant probing angles $\lambda_j \vec{\vartheta}_\Delta^{(j)}$. We find $\lambda_j \vec{\vartheta}_\Delta^{(j)}$ to be an excellent approximation for $\vec{\vartheta}_\Delta^{(j)}$.

Proof. For all points in the interior region, $Q_\sigma^\infty(\varphi, \vec{\theta}) = U_\sigma^\dagger(\vec{\theta}) Q_{3,\sigma}^\infty(\varphi) U_\sigma(\vec{\theta})$ for some symplectic unitary $U_\sigma(\vec{\theta})$ defined on the collective coordinate $X_{\sigma\varphi}$, due to Theorem A3. Define $U_{\pm\sigma}(\vec{\theta})$ as

$$U_{\pm\sigma}(\vec{\theta}) = \exp \left[i \left(\begin{array}{c} X_{\pm\sigma\varphi} \\ P_{\pm\sigma\varphi} \end{array} \right)^\dagger \Lambda \left(\begin{array}{c} X_{\pm\sigma\varphi} \\ P_{\pm\sigma\varphi} \end{array} \right) \right], \quad (\text{A1})$$

where $\Lambda = \Lambda^T$ specifies the symplectic transformation $U_\sigma(\vec{\theta})$, and $U_{-\sigma}(\vec{\theta})$ is defined with the same Λ but on the coordinate $X_{-\sigma\varphi}$. Notice also that we can relate the local and global coordinates as

$$\left(\begin{array}{c} X_{+\varphi} \\ X_{-\varphi} \\ P_{+\varphi} \\ P_{-\varphi} \end{array} \right) = \left[\mathbb{1} \otimes \underbrace{\left(\begin{array}{cc} \cos \varphi & \sin \varphi \\ -\sin \varphi & \cos \varphi \end{array} \right)}_{\mathcal{R}_\varphi} \right] \left(\begin{array}{c} X_1 \\ X_2 \\ P_1 \\ P_2 \end{array} \right), \quad (\text{A2})$$

and thus

$$\begin{aligned} &U_+(\vec{\theta}) U_-(\vec{\theta}) \\ &= \exp \left[i \left(\begin{array}{c} X_{+\varphi} \\ X_{-\varphi} \\ P_{+\varphi} \\ P_{-\varphi} \end{array} \right)^\dagger (\Lambda \otimes \mathbb{1}) \left(\begin{array}{c} X_{+\varphi} \\ X_{-\varphi} \\ P_{+\varphi} \\ P_{-\varphi} \end{array} \right) \right] \\ &= \exp \left[i \left(\begin{array}{c} X_1 \\ X_2 \\ P_1 \\ P_2 \end{array} \right)^\dagger (\mathbb{1} \otimes \mathcal{R}_\varphi^\dagger) (\Lambda \otimes \mathbb{1}) (\mathbb{1} \otimes \mathcal{R}_\varphi) \left(\begin{array}{c} X_1 \\ X_2 \\ P_1 \\ P_2 \end{array} \right) \right] \\ &= U_1 U_2, \end{aligned} \quad (\text{A3})$$

where $U_n = \exp[i(\frac{X_n}{P_n})^\dagger \Lambda(\frac{X_n}{P_n})]$ are now unitaries defined in the local coordinates. Therefore,

$$\begin{aligned} Q_\sigma^\infty(\varphi, \vec{\theta}) &= U_\sigma^\dagger(\vec{\theta}) U_{-\sigma}^\dagger(\vec{\theta}) Q_{3,\sigma}^\infty(\varphi) U_\sigma(\vec{\theta}) U_{-\sigma}(\vec{\theta}) \\ &= U_1^\dagger U_2^\dagger Q_{3,\sigma}^\infty(\varphi) U_1 U_2. \end{aligned} \quad (\text{A4})$$

Since the maximisation over the set of positive partial transpose states is unchanged under local unitary operations, we have $\mathbf{P}^{\infty\text{-sep}}(\varphi, \vec{\theta}) = \mathbf{P}_3^{\infty\text{-sep}}(\varphi)$ as desired. \square

Therefore, the Wigner function can be simplified to

$$\begin{aligned} W_{A(\vec{\theta})}(x, p) &= \frac{1}{2\pi K^2} \sum_{j=0}^{K-1} \sum_{k=0}^{K-1} \text{sgn}[x(\theta_j)x(\theta_k)] \text{si} \left| \frac{2x(\theta_j)x(\theta_k)}{\sin(\theta_j - \theta_k)} \right| \\ W_{A(\vec{\theta})}(r \cos \phi, r \sin \phi) &= \frac{1}{2\pi K^2} \sum_{j=0}^{K-1} \sum_{k=0}^{K-1} \text{sgn}[\cos(\phi - \theta_j) \cos(\phi - \theta_k)] \text{si} \left| \frac{2r^2 \cos(\phi - \theta_j) \cos(\phi - \theta_k)}{\sin(\theta_j - \theta_k)} \right|. \end{aligned} \quad (\text{A3})$$

Hence, $\text{tr}[A(\vec{\theta})^2]$ is

$$\begin{aligned} \text{tr}[A(\vec{\theta})^2] &= \frac{1}{16\pi^3 K^4} \int_{-\pi}^{\pi} d\phi \int_0^\infty d[r^2] \sum_{j=0}^{K-1} \sum_{k=0}^{K-1} \sum_{l=0}^{K-1} \sum_{m=0}^{K-1} \text{sgn}[\cos(\phi - \theta_j) \cos(\phi - \theta_k) \cos(\phi - \theta_l) \cos(\phi - \theta_m)] \\ &\quad \times \text{si} \left| \frac{2r^2 \cos(\phi - \theta_j) \cos(\phi - \theta_k)}{\sin(\theta_j - \theta_k)} \right| \text{si} \left| \frac{2r^2 \cos(\phi - \theta_l) \cos(\phi - \theta_m)}{\sin(\theta_l - \theta_m)} \right| \\ &= \frac{1}{64\pi^2 K^4} \int_{-\pi}^{\pi} d\phi \sum_{j=0}^{K-1} \sum_{k=0}^{K-1} \sum_{l=0}^{K-1} \sum_{m=0}^{K-1} \text{sgn}[\cos(\phi - \theta_j) \cos(\phi - \theta_k) \cos(\phi - \theta_l) \cos(\phi - \theta_m)] \\ &\quad \times \min \left\{ \left| \frac{\sin(\theta_j - \theta_k)}{\cos(\phi - \theta_j) \cos(\phi - \theta_k)} \right|, \left| \frac{\sin(\theta_l - \theta_m)}{\cos(\phi - \theta_l) \cos(\phi - \theta_m)} \right| \right\}. \end{aligned} \quad (\text{A4})$$

Now, the remaining integral involves an integrand that is the sum of piecewise smooth functions: apart from non-differentiable points whenever the sign function flips signs or the minimum function swaps between its arguments, the function is simply the reciprocal of two cosines, which is smooth within the nondifferentiable points.

We can therefore split the integral as $-\pi \leq \phi \leq \pi = \sum_{n=0}^{|\Phi|+1} \int_{\phi_n}^{\phi_{n+1}}$, where $\phi_0 = -\pi$, $\phi_{|\Phi|+1} = \pi$, and $\phi_n \in \Phi$

Appendix A7: Rigorous Upper Bound for Precession Protocol With More Angles

From Eq. (A2), the Wigner function of $A(\vec{\theta}) := (Q(\vec{\theta}) - \frac{K+1}{2K})(Q(\vec{\theta}) - \frac{K-1}{2K})$ for $KQ(\vec{\theta}) := \sum_{k=0}^{K-1} \Theta[X(\theta_k)]$ is

$$W_{A(\vec{\theta})}(x, p) = \frac{K^2 - 1}{4K^2} + \frac{1}{2\pi K^2} \sum_{j=0}^{K-1} \sum_{k=0}^{K-1} \text{si} \left[\frac{2x(\theta_j)x(\theta_k)}{|\sin(\theta_j - \theta_k)|} \right]. \quad (\text{A1})$$

For the region where $\mathbf{P}^c(\vec{\theta}) = (1 + 1/K)/2$, $(K - 1)/2$ of the angles are always on one side and $(K + 1)/2$ of the angles on the other, so $(K - 1)/2 \cdot (K - 1)/2 + (K - 1)/2 \cdot (K - 1)/2 = (K^2 - 1)/2$ of the terms $x(\theta_j)x(\theta_k)$ will be negative, for which

$$\text{si} \left[\frac{2x(\theta_j)x(\theta_k)}{|\sin(\theta_j - \theta_k)|} \right] = -\pi - \text{si} \left| \frac{2x(\theta_j)x(\theta_k)}{\sin(\theta_j - \theta_k)} \right|. \quad (\text{A2})$$

is the n th smallest element of the set

$$\begin{aligned} \Phi &= \left\{ \phi : |\phi| \leq \pi : \exists j, k, l, m : \cos(\phi - \theta_k) = 0 \right. \\ &\quad \left. \vee \pm \frac{|\sin(\theta_j - \theta_k)|}{\cos(\phi - \theta_j) \cos(\phi - \theta_k)} \right. \\ &\quad \left. = \frac{|\sin(\theta_l - \theta_m)|}{\cos(\phi - \theta_l) \cos(\phi - \theta_m)} \right\}. \end{aligned} \quad (\text{A5})$$

Here, Φ includes all points ϕ at which the sgn and min functions are nondifferentiable. Note that closed-form expressions of the elements of Φ can be found—the condi-

tion $\cos(\phi - \theta_k) = 0 \implies \phi = \theta_k + (2l+1)\pi/2$ for integer l , and the condition involving reciprocals can be rewritten into a quadratic polynomial of $\tan \phi$. This means that we can rewrite Eq. (A4) as a sum of integrals over smooth functions.

Within each integral, after taking care to use trigonometric identities to regulate the terms whose denominators go to zero in the same way as Eq. (A10), each integral

can be analytically evaluated to be

$$\begin{aligned} & \int_{\phi_n}^{\phi_{n+1}} d\phi \frac{\pm \sin(\theta_j - \theta_k)}{\cos(\phi - \theta_j) \cos(\phi - \theta_k)} \\ &= \pm \log \left[\frac{\cos(\phi_{n+1} - \theta_j) \cos(\phi_n - \theta_k)}{\cos(\phi_{n+1} - \theta_k) \cos(\phi_n - \theta_j)} \right]. \end{aligned} \quad (\text{A6})$$

This means that, in principle, closed-form solutions of Eq. (A4) can be evaluated analytically. In practice, however, the obtained expressions become very cumbersome for $K > 3$. Nonetheless, this shows that the value obtained from numerical integration of Eq. (A4) is reliable.

Finally, the expression $\text{tr}[A(\vec{\theta})^2] \geq 2[(\mathbf{P}^\infty(\vec{\theta}) - \frac{1}{2})^2 - (1/2K)^2]^2$ can be rearranged to find

$$\mathbf{P}^{\geq}(\vec{\theta}) := \frac{1}{2} \left(1 + \frac{1}{K} \sqrt{1 + 2K^2 \sqrt{2\text{tr}[A(\vec{\theta})^2]}} \right) \geq \mathbf{P}^\infty(\vec{\theta}). \quad (\text{A7})$$